Department of Engineering Physics and Mathematics
Helsinki University of Technology
FIN-02015 HUT, Finland

Doubly Quantized Vorticity and other NMR Experiments on Rotating ^{3}He Superfluids

Jaakko Ruohio

Low Temperature Laboratory

Helsinki University of Technology

Dissertation for the degree of Doctor of Science in Technology to be presented with due permission of the Department of Engineering Physics and Mathematics for public examination and debate in Auditorium F1 at Helsinki University of Technology (Espoo, Finland) on the 6th of April, 2001, at 12 o'clock noon.

Espoo 2001

Keywords: Quantum fluids, superfluid helium-3, quantized vortices, vortex arrays, vortex formation, vortex annihilation, nonlinear NMR, superfluid-superfluid interfaces, nuclear magnetic resonance, NMR spectrometer

Abstract

This doctoral thesis consists of experimental studies on rotating superfluid helium-3 at millikelvin temperatures. Superfluid ^{3}He provides an example of ordered systems where quantum phenomena are visible on a macroscopic scale. The order parameter is described by a 3×3 complex matrix leading to different superfluid phases with different properties. The A and B phases support topologically different kinds of defects, most notably vortex lines. Vortex lines are most easily created and studied in uniform rotation. Because of quantum nature, the circulation around the vortices is quantized in units of $\kappa_0 = h/2m_3$.

In superfluid ^{3}He nuclear magnetic resonance (NMR) provides a means to distinguish between different types of vortices and count them one by one. During the course of this work the sensitivity of the NMR spectrometer was improved by an order of magnitude, which enabled the direct measurement of the circulation of a vortex in the A phase that carries two circulation quanta ($2\kappa_0$). Up to now the circulation of the known quantized vortex types in other quantum fluids, which include superfluid ^{4}He, superconductors, and Bose–Einstein -condensates, has been singly quantized.

Other NMR experiments reported in the thesis are: (1) The first qualitative measurements of vortex annihilation in the A and B phases of ^{3}He. These measurements tell the lowest rotation velocity that stabilizes an array of vortex lines with a given number of vortices, and how it depends on the type of the defect. (2) Studies of vortex arrays with both singly and doubly quantized A phase vortex lines coexisting in the experimental container. ^{3}He-A provides a unique system in which this kind of arrangement can be done. (3) In order to improve the vortex detection sensitivity in the B phase even further, the response of different nonlinear spin precession modes to superfluid-normal fluid counterflow was studied. A new mode, where the orbital angular momentum is oriented transverse to the external magnetic field, was found.

ISBN 951-22-5392-5

Contents

1 Introduction **1**

1.1 Superfluidity in ^{3}He 1

1.2 Quantized vorticity 2

1.3 Comparison with other superfluids 3

2 Methodology **4**

2.1 Continuous-wave nuclear magnetic resonance spectroscopy 4

2.2 High quality factor resonators 5

2.2.1 Static susceptibility 6

3 Superfluid in rotation **7**

3.1 Equilibrium pattern of vortices 7

3.2 Annihilation of vortex lines 10

4 Nonlinear NMR modes in ^{3}He-B **16**

5 Direct observation of double quantization in ^{3}He-A **18**

6 Rotating A-B phase-boundary experiment **21**

6.1 Introduction 21

6.2 Earlier experiments on the A-B phase boundary 23

6.3 Design considerations 24

6.3.1 Choice of polarization fields for A and B phase NMR 24

6.3.2 Design of the NMR magnets 28

6.3.3 NMR pick-up coils 31

6.3.4 Thermometers 32

6.3.5 Instrumentation 32

6.4 Possible experiments 32

7 List of publications **36**

7.1 Author's own contribution 38

7.2 Other related publications 39

Acknowledgments **40**

References **41**

1 Introduction

1.1 Superfluidity in ^{3}He

Liquid ^{3}He is a quantum liquid at low temperatures. To explain its properties, quantum statistical mechanics is needed. The ^{3}He atom and the more common isotope of helium, ^{4}He, are light in mass, and the zero-point motion of atoms is so large that helium is the only element which does not solidify at the absolute zero temperature at ambient pressure. Remarkably, superfluidity is observed below a critical temperature T_c, when the fermionic ^{3}He atoms start to form Cooper pairs which are bosons. A macroscopic amount of these bound pairs condenses into the ground state, so they occupy the same quantum state described by a single wave function.

Since the Cooper pairs of ^{3}He have internal structure, spin and orbital degrees of freedom, the ordered state is described by a wave function with nine complex amplitudes. A consequence of this is the existence of different superfluid phases as a function of pressure, temperature, and magnetic field. The superfluid phases have different internal symmetries and therefore different physical properties.

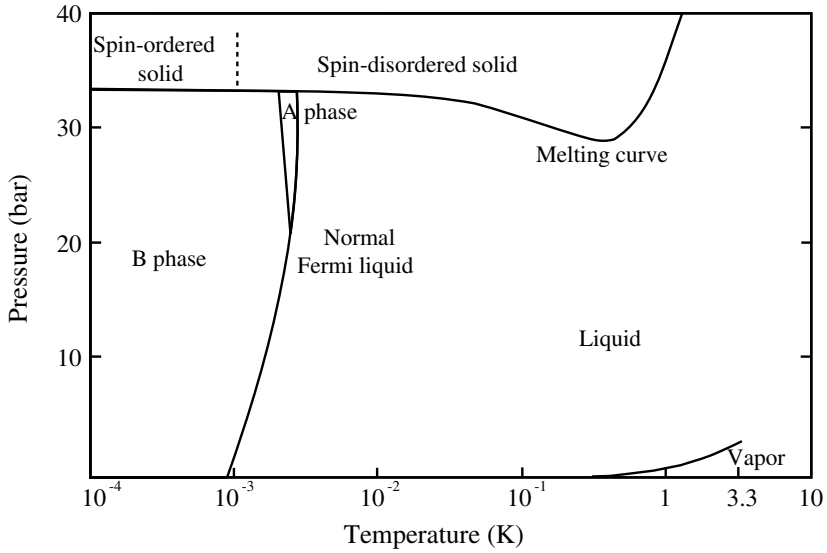

Figure 1: Phase diagram of ^{3}He in zero magnetic field. Two bulk superfluid phases, A and B, are stable at millikelvin temperatures [1]. A third one, A_1, is stabilized in a finite magnetic field.

The superfluid phases have a high degeneracy of equilibrium states described by an order parameter. Spatial variations of the order parameter describing the continuously degenerate equilibrium states are called textures. Mass flow results from gradients in

the order-parameter texture. Since a nonuniform texture can be the ground state of the ordered system, inhomogeneity cannot be a source for dissipation. This is the basis of frictionless flow of macroscopic amounts of atoms in superfluids [2]. Indeed, this is the "super" property of superfluids.

1.2 Quantized vorticity

Some defects in the order-parameter field, most notably vortices, are extremely stable due to the conserved charges induced by their topological properties. Uniform rotation is the simplest way to create vortices in large quantities and to study them systematically. So far seven different types of vortices have been experimentally observed, three in the B phase, and four in the A phase [3].

In classical hydrodynamics, vorticity is defined as the curl of the velocity field, $\nabla \times \mathbf{v}$. A vortex tube is a bunch of lines whose direction is that of the vorticity vector [4]. The strength of a vortex tube is measured in terms of the circulation

$$\kappa = \oint \mathbf{v} \cdot d\mathbf{r}. \tag{1}$$

In superfluids the size of the vortex tube is much smaller than any relevant hydrodynamical scale, and all the vorticity is concentrated in thin filaments, from here on called vortex lines. The circulation of superfluid vortex lines is quantized in units of κ_0 because of single-valuedness of the order parameter. The quantum of circulation in ^{3}He is $\kappa_0 = h/2m = 0.066\,\mathrm{mm}^2/\mathrm{s}$, where h is Planck's constant and m is the mass of a ^{3}He atom. But this is only the standard picture. In ^{3}He-A the superflow v_s is not necessarily potential and continuous vorticity can be supported without a singular vortex core. This kind of vortices carrying multiple quanta of circulation will be discussed in Sec. 5.

In the two-fluid model, the liquid is regarded as a mixture of a normal fluid component and a superfluid component. Once rotated at an angular velocity Ω, the viscous normal fluid component rotates with the bucket and

$$\nabla \times \mathbf{v}_n = \nabla \times (\mathbf{\Omega} \times \mathbf{r}) = 2\mathbf{\Omega}, \tag{2}$$

while the superfluid component remains at rest. When a critical flow velocity is reached, vortices appear in order to lower the free energy of the system. The movement of the vortex lines is the main energy loss mechanism in superfluids. Below the critical flow velocity mass can be transported without dissipation.

Low millikelvin temperatures require extensive cryogenic engineering, and up to now five rotating cryostats combining a nuclear demagnetization stage with a dilution refrigerator have been constructed. The first rotating cryostat, Rota I in Helsinki, became operational in 1981 and could be rotated at moderate speeds and was capable of reaching submillikelvin temperatures [5]. Other rotating cryostats have been built in Cornell [6], Helsinki [7], Berkeley [8], and Manchester [9].

In addition to rotation, vortices have been created in ^{3}He by using moving pistons, weak links [10], and at ultra-low temperatures by neutron irradiation [11], and vibrating wires [12].

1.3 Comparison with other superfluids

Superfluidity of ^{3}He has been studied extensively ever since it was discovered in 1972 [13]. Research on superfluid ^{3}He and its vortices has parallels with other coherent quantum systems.

The other known superfluid is ^{4}He. Its condensate consists of bosons having zero spin and zero orbital angular momentum. Therefore, there is only one superfluid phase, and one kind of a vortex with a singular normal-phase core. The importance of quantum statistics at low temperatures is displayed by the thousand times higher critical temperature for the superfluid transition in ^{4}He compared to that of ^{3}He.

Superconductors can be considered to be superfluids with their conduction electron fluid. Applying an external magnetic field in a superconductor corresponds to applying rotation in neutral superfluids. Likewise, quantized flux lines in superconductors correspond to quantized vortices in superfluids. Probing fundamental aspects of vortices is more difficult in superconductors because of impurities, pinning, and challenges in growing faultless single-crystal samples. Liquid ^{3}He, in contrast, is at low temperatures the purest substance known since impurities are adsorbed on the walls of the container.

Lately, there has been a lot of interest in new condensed matter systems, such as the Bose–Einstein condensates of alkali atoms [14]. Such a gaseous system was originally proposed by S. N. Bose and A. Einstein. Using a focused laser beam to stir a Bose–Einstein condensate of ^{87}Rb gas confined in a magnetic trap, the formation of vortices has been observed [15, 16].

Superfluid ^{3}He is the most complex coherent many-body system that is available for experimental studies in a laboratory setting. It serves as a model for other quantum systems [17] because experiments on ^{3}He usually have a successful theoretical description.

The reasons are that in a fermionic system only particles with energies close to the Fermi surface E_F need to be considered, and that the gap energy Δ is small compared to E_F.

Perhaps the most promising real world application of superfluids is a gyroscope for the detection of the earth's rotation $\Omega_\oplus$. The accuracy of $10^{-2}\Omega_\oplus$ has been achieved for a superfluid helium ^{4}He gyroscope utilizing phase-slippage techniques [18]. When developed, gyroscopes based on the Josephson effect in ^{3}He [10, 19, 20] are believed to improve the accuracy by many orders of magnitude becoming competitive with ring lasers. Also, there is some potential to build a sensitive weakly interacting massive particle detector using ^{3}He cooled to 100 μK temperatures [21].

2 Methodology

2.1 Continuous-wave nuclear magnetic resonance spectroscopy

Rotating superfluids have been studied with many techniques including gyroscopy, ultrasound attenuation, ion mobility, and optical methods. While all of these methods have brought valuable new information, nuclear magnetic resonance (NMR) is so far the most instrumental for both quantitative and qualitative studies about the vortex structures that are produced in the rotating ^{3}He superfluids.

In general, a phenomenon called magnetic resonance is found in systems possessing magnetic moments and angular momentum [22]. NMR spectroscopy can be applied to ^{3}He since the ^{3}He atom has a small nuclear moment $\mu = -3.56 \cdot 10^{-26}\,\mathrm{J/T}$, and a radio frequency (RF) field $\omega = \gamma H$, where the gyromagnetic ratio $\gamma/(2\pi) = 32.4\,\mathrm{kHz/mT}$, can excite the spins. In continuous wave NMR the sample is excited at a fixed frequency and the sample is driven into the resonance with a magnetic field. The signal is read, usually phase sensitively, with a lock-in amplifier, giving absorptive and dispersive components of the resonance curve.

By its very nature, NMR probes the spin system. Its usefulness for studies of ^{3}He in rotation arises from the coupling of the spin part of the order parameter to the orbital part via a spin-orbit interaction. In this way, information on the orbital texture can be retrieved using NMR.

Continuous wave NMR with small tipping angles is so far the most advanced way to investigate vortices in ^{3}He. The structure of vortex lines can be deduced in both the A and B phases [23, 24], and the number of vortex lines can be counted individually as they are nucleated [P11] and [25].

A pulsed measurement is commonly used in NMR, but for studies of rotating superfluid ^{3}He, the continuous wave method is better suited. In order to achieve high sensitivity in pulsed NMR, large tipping angles are required. Then the spin dynamic equations of Leggett [26] cannot be linearized, and nonlinear NMR modes such as a homogeneously precessing domain (HPD) can appear. In addition, large tipping angles are known to modify the orbital order parameter field, which is of main interest here. Moreover, in superfluid ^{3}He rather large frequency shifts from the Larmor frequency ω_L up to 5% can occur due to the spontaneously broken spin-orbit symmetry. The bandwidth of a tuned detection coil is f/Q which means that the detection would be in the so-called super-Q limit [27].

Thus we use the continuous-wave NMR method and have achieved high sensitivity using an LC-tank circuit with a high quality (Q) value.

2.2 High quality factor resonators

The continuous-wave NMR measurement is essentially a Q value measurement. The Q value of an LC-resonant circuit is defined by

$$Q = \frac{\omega L}{R}, \tag{3}$$

where ω is the resonance frequency, L is the inductance, and R represents the losses in the resonator. Sources of the losses can be accounted for by defining a conductor quality factor Q_c, a dielectric quality factor Q_d, a radiation quality factor Q_r, and an external quality factor Q_e from an external load [28]. The total unloaded quality factor is given by

$$\frac{1}{Q} = \frac{1}{Q_c} + \frac{1}{Q_d} + \frac{1}{Q_r} + \frac{1}{Q_e}. \tag{4}$$

Placing a sample inside the inductor changes the inductance by $L \rightarrow L(1 + \xi\chi)$, where ξ is the filling factor, and χ is a frequency dependent complex susceptibility of the sample. The output voltage u is detected phase sensitively with a constant excitation current flowing through the resonator

$$\frac{u - u_0}{u_0} = \frac{-iQ\xi\chi}{1 + iQ\xi\chi}, \tag{5}$$

where u_0 is the output signal of the resonator without the sample. Therefore, the lower the losses for the unloaded resonator, the higher the sensitivity of the resonator for the NMR detection of superfluid ^{3}He susceptibility will be. When $Q\xi\chi \sim 1$, the output signal is no longer linear, but high Q values are nevertheless desirable, especially for small signals.

Typically, the signal-to-noise ratio of a nuclear magnetic resonance measurement scales as $Q^{1/2}$.

A drastic improvement in Q_c follows from using a superconducting wire for the inductance L [29]. Usually this is not done since good polarizing field homogeneity is required, and it is somewhat perturbed by a superconductor close to the sample. However, in ^{3}He internal relaxation mechanisms, increasing towards decreasing temperatures, dominate the line width and thus justify the use of superconducting wire.

The external load Q_e arises from a cooled preamplifier working at temperatures of a few kelvins. The preamplifier is used for signal amplification and is needed for high impedance coupling to the tank circuit [29].

In publication [P1] the radiation quality factor Q_r was identified to be the largest source of losses originating from the induced currents in the low conductivity body of the polarizing NMR magnet. High-RRR copper cylinders inserted inside the magnet former and change of the pickup coil geometry allowed for an order-of-magnitude improvement in the Q value of the spectrometer from $Q = 2\,000$ to $Q = 25\,000$. Increased Q value and digital filtering of the data made the detection of a single vortex signal in the A phase possible [P11].

When high Q values are used, the measured signals are not linearly proportional to the absorption and the dispersion. The distortion from a high Q value can be corrected by solving χ from Eq. (5).

2.2.1 Static susceptibility

In publications [P2] and [P3] the dispersion signal was not available for the high Q correction. We show here that under certain conditions the static susceptibility can be obtained from the measured data without any correction for the high Q value. This is useful because, for example, in the A phase the number of vortices can be measured from the susceptibility of the so-called vortex satellite.

The static susceptibility is defined as [22]

$$\chi_0 = \chi'(0) = \frac{1}{\pi}\wp\int_{-\infty}^{+\infty}\frac{\chi''(\omega')}{\omega'}\,d\omega' \approx \frac{2}{\pi}\frac{1}{\omega_0}\int_0^{+\infty}\chi''(\omega')\,d\omega', \tag{6}$$

where $\chi(\omega) = \chi'(\omega) - i\chi''(\omega)$ are the dispersion and the absorption satisfying $\chi(-\omega) = \bar{\chi}(\omega)$, the bar denotes the complex conjugate, and $\wp$ means the principal value. The last approximation is valid when all the absorption occurs close to the resonance frequency ω_0. Obviously, Eq. (6) assumes that the NMR response is linear with respect to the RF

excitation.

Provided that $\max(|iQ\xi\chi|) < 1$ from Eq. (5) follows

$$\frac{1}{\xi Q}\int_0^{+\infty} \Re\left(\frac{u-u_0}{u_0}\right)\, d\omega' = \Re\int_0^{+\infty} \frac{i\chi}{1+iQ\xi\chi}\, d\omega' = \tag{7}$$

$$\Re\int_0^{+\infty} \left[i\chi + Q\xi\chi^2 - iQ^2\xi^2\chi^3 - \ldots\right]\, d\omega' = \tag{8}$$

$$\int_0^{+\infty} \chi''\, d\omega' + \int_0^{+\infty} Q\xi(\chi'^2 - \chi''^2)\, d\omega' + \ldots. \tag{9}$$

From the Kramers–Kronig relation it follows that the asymptotic form of the dispersion far from resonance is

$$\chi'(\omega) = \frac{\chi_0\omega_0}{2}\left(\frac{1}{\omega+\omega_0} - \frac{1}{\omega-\omega_0}\right). \tag{10}$$

Using this formula, an error estimate for χ_0 can be calculated from the second-order term in Eq. (9) assuming that the measurement is carried out on the interval $(\omega_0-\Delta\omega, \omega_0+\Delta\omega)$

$$-\int_{\omega_0-\Delta\omega}^{\omega_0+\Delta\omega} Q\xi(\chi'^2 - \chi''^2)\, d\omega' \approx \int_0^{\omega_0-\Delta\omega} Q\xi\chi'^2\, d\omega' + \int_{\omega_0+\Delta\omega}^{\infty} Q\xi\chi'^2\, d\omega' \approx \frac{Q\xi\chi_0^2\omega_0^2}{2\Delta\omega}, \tag{11}$$

where Parseval's theorem has been used and $\Delta\omega \ll \omega_0$ has been assumed. Thus, provided that

$$\frac{Q\xi\chi_0\omega_0}{\pi\Delta\omega} \ll 1, \tag{12}$$

the static susceptibility can be obtained to a good approximation from the measured data by integrating it directly without any corrections for the high Q value.

For the ^{3}He Fermi liquid, the static susceptibility can obtain values $\chi_0 = 4.8\cdot10^{-7} - 1.4\cdot10^{-6}$ depending on pressure [30]. The integrated signals from the vortices in the A phase can be five times lower than χ_0, or even less. Values of $Q = 2000-25000$ have been obtained in our experiments and the filling factors have typically been a few percent.

3 Superfluid in rotation

3.1 Equilibrium pattern of vortices

The response of a superfluid to rotation is the formation of an array of quantized vortex lines parallel to the axis of rotation. The array simulates solid-body rotation globally minimizing the free-energy function

$$F = E - L\Omega, \tag{13}$$

where E is the total kinetic energy in the superfluid motion, L is its angular momentum, and Ω is the rotation velocity of the container.

For an isotropic superfluid the equilibrium pattern of rectilinear vortex lines in a rotating cylinder is obtained from the minimization of the free energy per unit length [31]

$$f = -\sum_{i<j} \ln|z_i - z_j|^2 + \frac{1}{2}\sum_{i,j} \ln|1 - z_i\bar{z}_j|^2 - \omega\sum_i (1 - |z_i|^2) + N\ln(R/a). \qquad (14)$$

Reduced units are used, such that $f = 4\pi F/(\rho\kappa^2)$, $\omega = (2\pi R^2/\kappa)\Omega$, and $z_i R$ are the complex positions of the vortex cores. Above, R is the container radius, ρ is the density of the superfluid, a is the vortex-core radius, and κ is the circulation quantum. The first term in Eq. (14) takes into account the interaction between the vortex lines. The second term ascribes to the interaction between the vortex lines and the image vortices at $1/\bar{z}_i$. The image vortices with negative circulation are needed to fulfill the circular boundary condition so that the flow is perpendicular to the normal of the wall. The third term is proportional to the rotation velocity ω and it accounts for the angular momentum of the fluid. The fourth term describes the intrinsic energy of the vortex lines $\ln(R/a)$. The intrinsic energy is here taken not to depend on the vortex density.

For a given vortex number N, the vortex pattern is numerically obtained by starting from an initial guess, and then moving the vortices along the negative gradient of the free energy

$$u_k = -\frac{1}{2}\partial f/\partial\bar{z}_k = \sum_{j\neq k} \frac{1}{\bar{z}_k - \bar{z}_j} - \sum_j \frac{1}{\bar{z}_k - 1/z_j} - \omega z_k \qquad (15)$$

until $u_k \approx 0$. The local energy minima for 23 vortices are shown in Fig. 2. The ring numbers are shown to identify the configurations, and the slight difference in energy compared to the pattern 23_1 is also shown.

At large rotation velocities, the array is dense and in the center it optimally has triangular symmetry. Circular distortion on outer rings is due to rotational symmetry and it is present in the absence of a circular boundary condition as well. In the lattice the superfluid component velocity matches on the average the normal fluid component velocity. On the container wall the counterflow $v_n - v_s$ is highest, reaching a value of $(\omega - N)\kappa/(2\pi R)$ on the average. Azimuthally averaged flow velocities as a function of radius are shown in Fig. 3.

Numerical determination of rotational equilibrium states of an irrotational fluid [31] was motivated by the superfluidity of ^{4}He. In ^{4}He at 100 mK the vortex patterns up to $N = 11$ vortices have been photographed in the Berkeley experiments [32]. Because lower

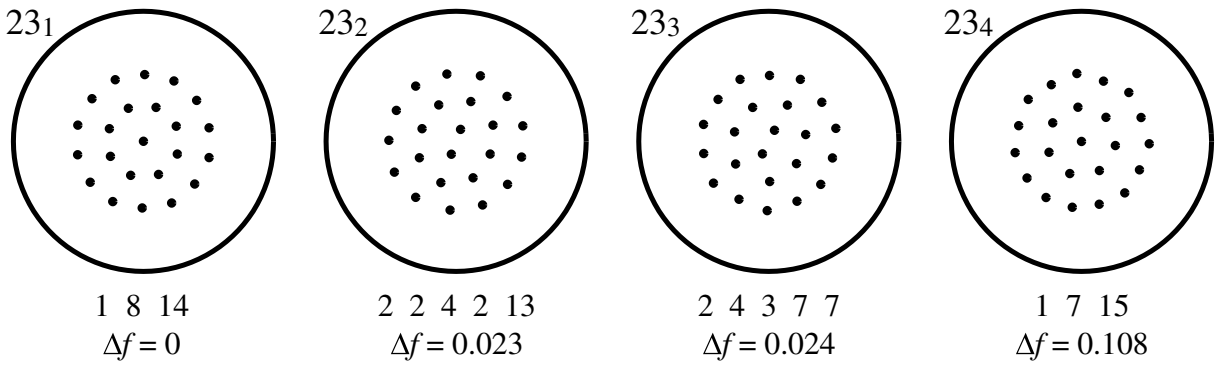

Figure 2: Stationary vortex patterns of 23 singly quantized vortex lines at a rotation velocity $\omega = 58$ in units of $\kappa/(2\pi R^2)$. All patterns are locally stable, and are shown in the order of increasing energy f using the Los Alamos Catalog labeling [31]. Pattern 23_1 has the lowest energy, and would be the equilibrium configuration for vortex line energy $\ln(R/a) = \ln 10^7$ in units of $\rho\kappa^2/(4\pi)$. The occupation of the various concentric rings are shown below the configuration. The energy differences are huge compared to the experimental temperatures. For example, $f = 1$ corresponds to a temperature per unit length of the order of $10^9\,\mathrm{K/m}$ for helium superfluids.

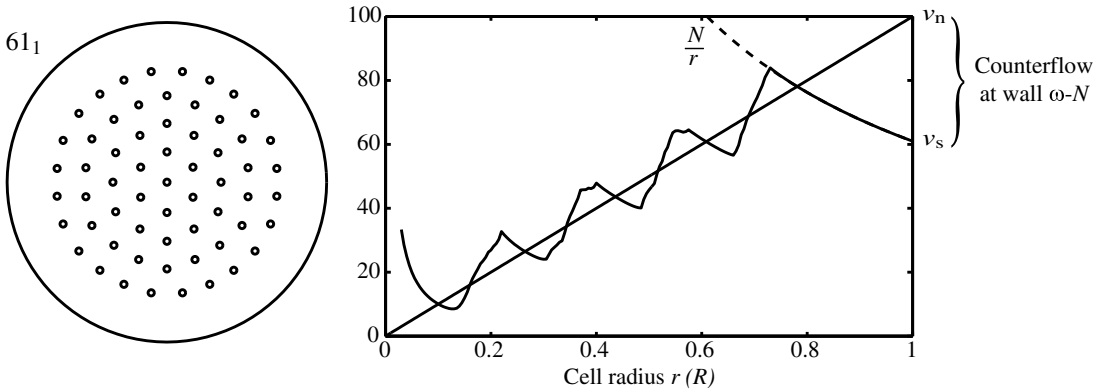

Figure 3: Average superfluid component and normal component velocities as functions of radius for the pattern 61_1 at $\omega = 100$. On the wall $r = R$, the counterflow reaches the highest value of $\omega - N$. Experimentally, this kind of situation could arise for $N = 61$ doubly quantized A-phase vortices with a critical velocity higher than $2\kappa_0(\omega - N)/2\pi R = 0.41\,\mathrm{mm/s}$ in a cell with radius $R = 2\,\mathrm{mm}$ rotating at $\Omega = 526\,\mathrm{mrad/s}$.

temperatures are required, direct observation of the vortex lattice in ^{3}He superfluids has not yet been tried.

However, in ^{3}He-A the question of equilibrium patterns is more involved because vortices with different quantizations exist, namely $n = 1$ and $n = 2$. These singly and doubly quantized vortices can exist simultaneously in the experimental container. The experimental phase diagram of vortices as a function of rotation velocity and magnetic field that agrees with theory has been presented in Ref. [23]. We were able to resolve the radial distribution of singly and doubly quantized vortices experimentally from the NMR response to slow deceleration. The methods to create such states along with numerical studies are discussed in publications [P2] and [P3]. In ^{3}He-A the force balance equation for a moving vortex takes into account the anisotropic mass of the superfluid [33]. The doubly quantized vortices have a $1/r$ velocity field outside the soft vortex core [see Sec. 5, Eq. (30)]. Provided the soft cores of the $n = 2$ vortices do not overlap, the free-energy gradient Eq. (15) can be used to find the the equilibrium vortex patterns. At equilibrium the normal fluid velocity v_n and the superfluid velocity v_s are equal at the positions of the vortices.

Often a superfluid is in its equilibrium state only when it has been adiabatically cooled through the critical temperature T_c under constant rotation [34]. It is not only the energy consideration, but also the nucleation and annihilation mechanisms of vortex lines that determine the number of lines in the container. A rough estimate for the critical velocity is obtained from Eq. (15). If the position of a vortex line has to be at least a distance of order the radius of its core a from the wall, then

$$\omega_c = R/2a. \tag{16}$$

Experimentally in ^{3}He the critical velocity can be observed from an onset of a periodic stepwise change in the NMR spectrum as the rotation velocity is increased linearly. A hierarchy of critical velocities based on the vortex core size has been observed between vortices in ^{4}He, ^{3}He-B, and ^{3}He-A [35]. The stepwise change in the NMR signal was first observed in the B phase [36] and then in the A phase for the $n = 2$ vortices, as described in publications [P11] and [P12].

3.2 Annihilation of vortex lines

The rotation of the cylindrical container with an angular velocity ω stabilizes the vortex configuration. Upon deceleration an instability appears, where some vortices are lost to the boundary. This is called vortex annihilation.

In a two-dimensional framework, the intrinsic stability of a vortex pattern can be calculated from the Hessian of the vortex free energy in Eq. (14)

$$H = \begin{bmatrix} h_{11} & \cdots & h_{1N} \\ \vdots & \ddots & \\ h_{N1} & & h_{NN} \end{bmatrix} \tag{17}$$

where

$$h_{kj} = \begin{bmatrix} \frac{\partial^2 f}{\partial x_k \partial x_j} & \frac{\partial^2 f}{\partial x_k \partial y_j} \\ \frac{\partial^2 f}{\partial y_k \partial x_j} & \frac{\partial^2 f}{\partial y_k \partial y_j} \end{bmatrix} \tag{18}$$

and where $z_k = x_k + iy_k$. In this framework harmonic approximation is used and higher than second-order terms are neglected [37]. Now the problem is to calculate the $2N$ real eigenvalues of H. The $2N$ eigenvectors of H correspond to transverse normal vortex modes [38]. When the rotation velocity ω is decreased, mode softening occurs, and the first eigenvalue becoming negative marks the lower limit of absolute stability of the vortex pattern against annihilation, denoted by ω^*. The mode flow as a function of ω is calculated first by finding the vortex pattern using Eq. (15), and then the eigenvalue spectrum is calculated from the matrix H. An example of mode flow is presented in Fig. 4 for the pattern 61_2. All patterns have a Goldstone mode corresponding to pure rotation with a eigenvalue zero because of rotation symmetry in the problem. When searching for the first negative eigenvalue, one should not be confused with the Goldstone eigenvalue that might be numerically slightly negative. Some patterns like 14_2, 15_1, and 37_3 have shear modes corresponding to relative rotation of neighboring incommensurate rings and an eigenvalue $\lambda \approx 0$. Previously only values of ω^* for patterns 2_1, 3_1, 4_1, 5_1, 6_2, and 7_1 have been published [38]. These numerical calculations agree with the analytic solutions of the stability of patterns calculated by Havelock in 1931 [39] for 2_1, 4_1, and 6_2 while they fail for the patterns 3_1 and 5_1 (see footnote in Ref. [37]).

More values for ω^* have been calculated, and they are presented in Table 1. Patterns not found in Ref. [31] are labeled with letters, as the patterns cannot be ordered with increasing energy for all rotation velocities in the case of a circular boundary. For example, 61_2 becomes the global energy minimum below $\omega = 68.81$. We feel that values for ω^* give a good estimate on the annihilation instability because the energy barriers between different vortex patterns are large compared to the experimental millikelvin temperatures. Also, there is the question which transverse modes are excited in the experiments since as seen from Fig. 4, the pattern 61_2 is numerically stable below ω^*. We infer that when only a Magnus force Eq. (15) determines the motion of the vortex lines, a stable vortex system

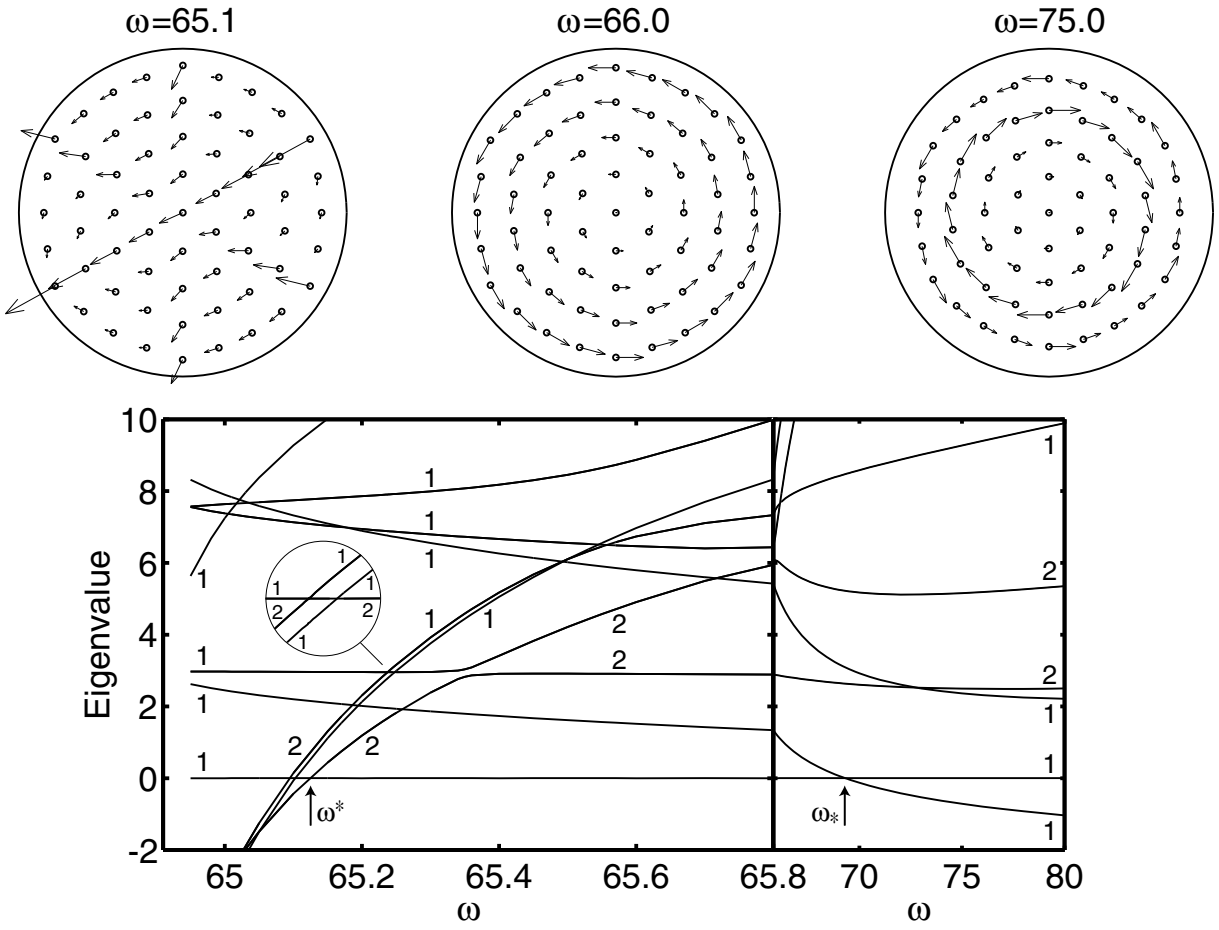

Figure 4: Mode flow for vortex pattern 61_2 at constant vortex number $N = 61$. Numbers in the figure show the degeneracy of the modes. At $\omega^* = 65.124$ the eigenvalues of two degenerate modes become negative and the local energy minimum transforms to a saddle point. The appearance of the saddle points below ω^* marks the lower limit of stability for the vortex pattern. As an example of reconfiguration, for rotation velocities higher than $\omega_* = 69.315$ this pattern becomes unstable and would transform to the global minimum energy pattern 61_1. The mode with $\lambda = 0$ is a Goldstone mode and is not physically interesting. Note the change in the scale of the ω axis at $\omega = 65.8$. Out of the 122 eigenvalues only the lowest are shown. On top of the figure the lowest eigenmode for three different velocities is shown.

Label	Ring numbers	ω^*	ω_*	Reconfiguration	Label	Ring numbers	ω^*	ω_*	Reconfiguration
1_1	1	1.000	-		30_4	4, 9, 17	33.23		
2_1	2	2.788	-		30_5	3, 3, 3, 7, 17	32.89		
3_1	3	3.575	-		37_1	1, 6, 6, 6, 18	50.19		$\omega^* \rightarrow 37_2$
4_1	4	4.693	-		37_2	1, 6, 6, 6, 18	39.81	51.58	$\omega_* \rightarrow 37_1$
5_1	5	5.933	-		37_3	1, 7, 12, 17	41.04	-	
5_2	1, 4	6.580	-		37_4	1, 6, 11, 19	46.15		$\omega^* \rightarrow 37_1$
6_1	1, 5	6.850	-		44_1	2, 8, 14, 20	54.05	-	$\omega^* \rightarrow 44_2$
6_2	6	8.373	-		44_2	2, 8, 14, 20	47.98	54.83	$\omega_* \rightarrow 44_1$
7_1	1, 6	7.550	-		50_1	4, 10, 15, 21	54.1		
8_1	1, 7	8.608	-		50_2	4, 9, 16, 21	58.2		$\omega^* \rightarrow 50_d$
15_1	4, 11	16.82	-		50_5	4, 4, 6, 16, 20	54.7		
15_2	5, 10	29.23	-	$(\omega^* \rightarrow 15_a)$	50_6	3, 3, 6, 9, 6, 23	54.2		
15_3	5, 10	17.10	27.58	$(\omega_* \rightarrow 15_a)$	50_a	2, 2, 8, 2, 14, 22	53.8	71.2	
15_a	5, 10	27.59	29.22	$\omega^* \rightarrow 15_3$, $\omega_* \rightarrow 15_2$	50_b	2, 2, 8, 2, 14, 2, 20	56.3	-	$\omega^* \rightarrow 50_e$
23_1	1, 8, 14	25.97	-		50_c	4, 9, 15, 22	54.6		
23_2	2, 2, 4, 2, 13	25.97	-		50_d	3, 1, 9, 1, 15, 21	54.0	-	
23_3	2, 2, 2, 3, 14	25.91	-		50_e	2, 2, 8, 2, 14, 2, 20	53.5	56.2	$\omega_* \rightarrow 50_b$
23_4	1, 7, 15	26.13	-		61_1	1, 6, 12, 18, 24	68.3		$\omega^* \rightarrow 61_2$
30_1	4, 4, 6, 16	32.77			61_2	1, 6, 12, 18, 24	65.2	69.3	$\omega_* \rightarrow 61_1$
30_2	4, 11 ,15	33.10			61_a	1, 6, 13, 17, 24	72.9		$\omega^* \rightarrow 61_1$
30_3	5, 5, 5, 15	34.88		$\omega^* \rightarrow 30_1$	61_b	1, 7, 12, 18, 23	65.6		

Table 1: Absolute stability limits for different vortex patterns. Patterns above ω^* and below ω_* are absolutely stable. Velocity ω^* marks the first instability against vortex annihilation or pattern reconfiguration, while ω_* marks the first instability against pattern reconfiguration. Ring numbers to identify the patterns and in some cases reconfigurations are also given.

does not necessarily occupy a local minimum of free energy. It is expected [37] that a small mutual friction term makes an energy minimum both necessary and sufficient for a stable vortex array. However, third-order terms in the free energy, which are neglected here, may become important when considering thermal fluctuations for some specific patterns, like 23_2, since they can make the energy barrier vanishingly small. Adding a longitudinal term to Eq. (15) enabled one to find the pattern 50_e which survives to the lowest rotation velocities out of the patterns with $N = 50$ vortices.

The measurements in publications [P4], [P5], and [P6] provide the motivation for this extended numerical study. In these annihilation experiments the velocity of the sample container is decreased and the number of vortices is measured. At high rotation velocities the number of vortex lines falls to the equilibrium curve upon deceleration because extrinsic annihilation mechanisms such as the nonalignment of the cell with respect to the rotation axis are dominant. Such equilibrium states can be used to measure line energies of quantized vortices. Below a cross-over velocity $\Omega^\dagger$, the number of vortex lines deviates from the equilibrium state. A closeup of the experimental results for singular vortices in the B phase is presented in Fig. 5.

A rough estimate for the intrinsic annihilation limit is presented in [P6], modified from a barrier calculation for vortices entering the cell given in Ref. [40]. This continuum model yields $\omega^* = N + 2\sqrt{N}$, which at small vortex numbers is flawed because the discrete two-dimensional model considering transverse vortex modes gives even lower values as shown in Fig. 5. The thin solid line should be on the left side of the stars because if the barrier vanishes for one vortex, the corresponding transverse vortex mode must also have a negative eigenvalue. The main reason for the failure is that the counterflow is assumed to be $v_n - v_s = \omega r - N/r$ throughout the entire counterflow region. Close to the vortex bundle this only holds on the average.

The measurements that were carried out in the same cell give remarkably different behavior for singular vortices in ^{3}He-B, singular vortices in ^{3}He-A, and continuous vortices in ^{3}He-A (see [P5]). In particular, for the continuous vortices in the A phase no deviation from the equilibrium state down to the lowest measured velocities is observed. In these measurements the rotation velocity is kept constant for a long time needed to record the whole spectrum. Since the two-dimensional discrete model based on the eigenvalues of the transverse modes gives too low values for ω^* and it does not distinguish between different types of vortices, a three-dimensional model of vortex modes with discrete lines is called for. Such a model is beyond the scope of this introductory treatise. However, if longitudinal modes of oscillations of vortex lines lead to annihilation, then necessarily

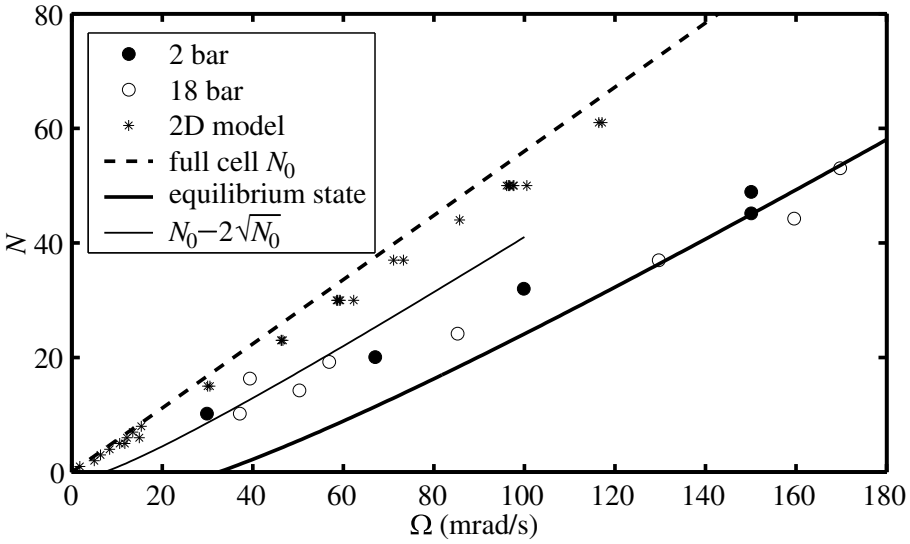

Figure 5: Annihilation threshold in ^{3}He-B at two different pressures, a closeup of Fig. 6 in [P6] shown below the cross-over velocity $\Omega^\dagger = 180\,\mathrm{mrad/s}$. The stars denote the transverse mode instability calculated and tabulated in Table 1. A simple model presented in Sec. 3 of [P6] for an instability against vortex annihilation gives $N = N_0 - 2\sqrt{N_0}$, where $N_0 = 560\Omega\,(\mathrm{rad/s})^{-1}$ corresponds to the number of vortices in a full cell. Since the intervortex distance is the only relevant length scale in the problem, the data are fitted into a function of the form $\alpha(\Omega - \beta\sqrt{\Omega})$. When comparing results from different experimental cells, the quantity to look at is βR.

this theory involves vortex line tension (see Ref. [4] for discussion). For the measured line types the vortex line tension is lowest for the continuous unlocked vortex in ^{3}He-A and highest for the singular vortex in ^{3}He-B. A three-dimensional model should most likely also take into account the experimentally inevitable noise in the rotation drive and vortex pinning and bending. Vortex pinning in ^{3}He has been studied in Ref. [41]. In conclusion, the measured points lie between the equilibrium line and the lower limits set by the two dimensional stability analysis as is expected, but the lowest measured points cannot be assigned to intrinsic instability of vortex lines against annihilation.

Vortex annihilation phenomena outside superfluid physics is interesting in the study of dynamics of pulsars. Pulsars are considered to be rotating neutron stars where the neutrons comprise a fermionic system with a degeneracy temperature of 10^{11} K, while the temperature of the star is estimated to be 10^8 K [42]. Most of the rotational energy of the neutron star can be in the neutron superfluid. Measurements of the rotation velocity of pulsars show a slow decrease as a function of time. Sometimes, abrupt speedups are observed, and models incorporating vortices to explain these glitches have been presented [43].

4 Nonlinear NMR modes in ^{3}He-B

The spin dynamics in superfluid ^{3}He are described by the Leggett equations [26]. These can be written for the B phase in a form that describes the motions of the magnetization $\mathbf{M}$ and the order parameter rotation matrix $\overleftrightarrow{\mathrm{R}}(\hat{\mathbf{n}}, \theta)$ [44]

$$\dot{\mathbf{M}} = \gamma \mathbf{M} \times \mathbf{H} + \frac{4}{15}\Omega_B^2 \frac{\chi}{\gamma} \sin\theta\,(1 + 4\cos\theta)\hat{\mathbf{n}}, \tag{19}$$

$$\dot{\hat{\mathbf{n}}} = -\frac{1}{2}\frac{\gamma}{\chi}[\hat{\mathbf{n}} \times (\mathbf{M} - \chi\mathbf{H}) + \cot\frac{\theta}{2}\,\hat{\mathbf{n}} \times (\hat{\mathbf{n}} \times (\mathbf{M} - \chi\mathbf{H}))], \tag{20}$$

$$\dot{\theta} = \frac{\gamma}{\chi}\hat{\mathbf{n}} \cdot (\mathbf{M} - \chi\mathbf{H}), \tag{21}$$

Here γ is the gyromagnetic ratio, $\mathbf{H}$ is the magnetic field, Ω_B is the longitudinal resonance frequency, and χ is the static susceptibility. The magnetic field usually consists of a static polarization component H_0 and a small time-dependent excitation component. The magnetization is related to the total spin density $\mathbf{S}$ by $\mathbf{M} = \gamma\mathbf{S}$. In the B phase, the order parameter is given by

$$A_{\mu j} = \Delta(T, p)\mathrm{e}^{i\phi} R_{\mu j}(\hat{\mathbf{n}}, \theta), \tag{22}$$

where Δ is the gap amplitude, ϕ is the overall phase variable and $\overleftrightarrow{\mathrm{R}}$ describes the combined rotations of the spin and orbital spaces [1]. So, the B phase is sensitive only to relative

rotations of the spin and orbital frames by an angle θ about an axis oriented along the unit vector $\hat{\mathbf{n}}$. Publication [P12] discusses $(\hat{\mathbf{n}}, \theta)$ textures under high counterflow in a rotating cylindrical container. The phase variable ϕ determines the mass-flow velocity

$$\mathbf{v}_s = \frac{\hbar}{2m_3}\nabla\phi, \tag{23}$$

and it can be solved from the conservation of the mass current $\nabla\cdot\mathbf{j}_s = 0$ and the boundary conditions, once $\mathbf{v}_s$ is known [45].

Spin dynamics in the B phase exhibits more features than in A phase. In the A phase the motion of the orbital anisotropy axis $\hat{\mathbf{l}}$ at finite temperatures is overdamped because of coupling of $\hat{\mathbf{l}}$ to the quasiparticle system [1]. The Leggett–Takagi spin-dynamic equations in ^{3}He-B taking into account relaxation terms have many nonlinear solutions and correspondingly many stable dynamic order-parameter states. In the case of small tipping angles, the equations can be linearized and the conventional NMR response is obtained that is linear in the RF excitation and independent of the field sweep direction. Experimentally, nonlinear NMR modes are pronounced when the RF excitation level is increased and the lineshapes become dependent on the direction of the field sweep. Observed nonlinear NMR modes can be identified by comparing them to analytical and numerical solutions for the Leggett–Takagi equations.

If the dipolar energy, giving rise to to the dipolar torque in Eq. (19), is averaged out over the period of precession, local minima in energy can be found where the magnetization has a nonequilibrium value. Half-magnetization states are an example of such states with $|\mathbf{M}| = \frac{1}{2}\chi H_0$ [46]. In these states, the order parameter axis $\hat{\mathbf{n}}$ precesses with half the frequency of precession of the magnetization $\mathbf{M}$, and a component with this frequency appears in the motion of $\mathbf{M}$ as well, as has been verified experimentally [47].

Whether vortex lines or vortex-free counterflow would have an effect on this kind of NMR modes was studied in publication [P7], but the answer was negative. The homogeneously precessing domain (HPD) still remains the most proficient in the study of vortex lines out of the many dynamic order-parameter states [48, 49] since vortex lines cause additional dissipation in HPD, which depends on the type of the lines. However, in the course of this study new NMR modes were found and once created at temperatures $0.98T_c < T < T_c$, all states proved to be unusually stable and could be cooled to below $0.7T_c$. The condition for the validity of averaging the dipole torque is $\Omega_B \ll \gamma H$, which means that the spin-orbital energy should be small compared to the Zeeman energy [50]. In that case, the system of order parameter vectors $\hat{\mathbf{d}}(\hat{\mathbf{k}}) = \overleftrightarrow{\mathrm{R}}(\hat{\mathbf{n}}, \theta)\hat{\mathbf{k}}$, where $\overleftrightarrow{\mathrm{R}}$ is a rotation matrix, moves as a single whole with respect to $\mathbf{H}$. At higher magnetic fields the condition

$\Omega_B \ll \gamma H$ is better fulfilled, and the stability regimes were found to be more extended at a field of 21.2 mT than in previous measurements with the same setup at 10.2 mT [46]. As the temperature is lowered, the Leggett–Takagi relaxation and the frequency shifts increase rapidly, and RF excitation fields comparable to or exceeding the equivalent of the dipole interaction need to be used as the states do not correspond to the true minimum of the dipole energy like the HPD does, for example.

An experimental cell made of quartz with smooth walls makes the critical velocity for vortex nucleation in the B phase [35] higher than the maximum rotation velocity of the cryostat $\Omega_{\max} = 3.5\,\mathrm{rad/s}$. Then at a high rotation velocity Ω in the vortex-free state, the effect of the counterflow $v_n - v_s$ on the orientation of the orbital angular momentum $\mathbf{L}$ by far exceeds that of the dipole coupling, whereas classically the orientations of $\mathbf{L}$ and $\mathbf{H}$ are parallel. While the cryostat is at rest, the NMR shows linear behavior, but starts to show nonlinearity as the rotation velocity is increased. This superflow-stabilized nonlinear NMR is discussed in publication [P8].

5 Direct observation of double quantization in ^{3}He-A

Unlike the other superfluids, ^{3}He-B and ^{4}He, superflow in ^{3}He-A is not potential but can be expressed with the help of an orthonormal set of unit vectors $(\hat{\mathbf{m}}, \hat{\mathbf{n}}, \hat{\mathbf{l}})$ as

$$\mathbf{v}_s = \frac{\hbar}{2m_3} \sum_i m_i \nabla n_i. \tag{24}$$

The complex vector $\hat{\mathbf{m}} + i\hat{\mathbf{n}}$ is the orbital part of the order parameter. Vectors $\hat{\mathbf{m}}$ and $\hat{\mathbf{n}}$ define the direction of the Cooper pair orbital angular momentum $\hat{\mathbf{l}} = \hat{\mathbf{m}} \times \hat{\mathbf{n}}$. The spin degrees of freedom of equilibrium states are described by an unit vector $\hat{\mathbf{d}}$ indicating the direction of the spontaneous magnetic anisotropy [2].

From Eq. (24) follows the Mermin–Ho relation [51]

$$\nabla \times \mathbf{v}_s = \frac{\hbar}{4m_3} \sum_{ijk} e_{ijk} l_i \nabla l_j \times \nabla l_k. \tag{25}$$

Thus since three-dimensional rotations do not commute, superflow in ^{3}He-A is not generally irrotational, but it can be, for example when the $\hat{\mathbf{l}}$ texture is confined to a plane.

The circulation number now becomes

$$n = \frac{2m_3}{h} \oint \mathbf{v}_s \cdot d\mathbf{r} = \frac{1}{2\pi} \int \hat{\mathbf{l}} \cdot \frac{\partial \hat{\mathbf{l}}}{\partial x} \times \frac{\partial \hat{\mathbf{l}}}{\partial y}\, dx\, dy, \tag{26}$$

where the first integral is around the core of the vortex along the boundary of a primitive cell in the vortex lattice and it counts the number of complete rotations of $(\hat{\mathbf{m}}, \hat{\mathbf{n}})$ about $\hat{\mathbf{l}}$. The second integral is over the vortex core and it measures the net area of the unit sphere that $\hat{\mathbf{l}}$ sweeps over the core. So it is possible to support vorticity in ^{3}He-A without a singularity in the order-parameter field.

Indeed, it turns out that in ^{3}He-A continuous vortices are possible and they are the prominent form of vorticity because they have the lowest critical velocity. A possible structure of the orbital part of the order parameter for a continuous high-field vortex with $n = 2$ has the parametrization [1]

$$\hat{\mathbf{d}} = \hat{\mathbf{y}} \tag{27}$$

$$\hat{\mathbf{l}} = \sin\eta(r)\,\hat{\mathbf{y}} \pm \cos\eta(r)[\sin\varphi\,\hat{\mathbf{x}} - \cos\varphi\,\hat{\mathbf{z}}] \tag{28}$$

$$\hat{\mathbf{m}} + i\hat{\mathbf{n}} = \mathrm{e}^{-i\varphi}[\sin\eta(r)(-\sin\varphi\,\hat{\mathbf{x}} + \cos\varphi\,\hat{\mathbf{z}}) \pm \cos\eta(r)\,\hat{\mathbf{y}} + i(\sin\varphi\,\hat{\mathbf{z}} + \cos\varphi\,\hat{\mathbf{z}})], \tag{29}$$

$$\mathbf{v}_s = \frac{\hbar}{2m_3 r}[1 + \sin\eta(r)]\,\hat{\boldsymbol{\varphi}}, \tag{30}$$

where η is a function of radius r such that $\eta(r \ll \xi_D) = -\frac{1}{2}\pi$ and $\eta(r \gg \xi_D) = \frac{1}{2}\pi$. In the A phase the dipolar length $\xi_D = 10\,\mu$m. This structure is dipole-unlocked, since above the dipolar field H_D the orientating effect of the magnetic field is stronger than the tiny spin-orbit coupling trying to lock the vectors $\hat{\mathbf{l}}$ and $\hat{\mathbf{d}}$ parallel or antiparallel. One structure based on a numerical calculation in Ref. [52] is depicted in Fig. 6.

The continuous high-field vortex was first observed in Ref. [53] and theoretical support to explain these as actual continuous vortices was presented in Ref. [54]. The identification of the quantization and the structure of the vortex lines arises from the comparison of the NMR response with theoretical calculations on vortex structures. The most recent calculations on different structures in the A phase can be found in Ref. [52].

Already before the first experiments, several questions arose, such as how to distinguish the signal from the vortices from the other signals caused by rotation and whether linear velocity dependence is sufficient evidence for the signal to arise from vortices. Here we have measured the NMR response of the dipole-unlocked vortex with improved resolution and determined the quantization of the double-quantized vortex structure directly for the first time and thus confirmed that the observed NMR satellites really arise from vortex lines. This requires better sensitivity in the A phase by an order of magnitude, than in the B phase because the origins of the NMR signals for vortex detection are different.

The linear increase in the signal above the critical rotation velocity Ω_c arises because new vortex lines are formed periodically, whenever v_c is reached. The expression for the

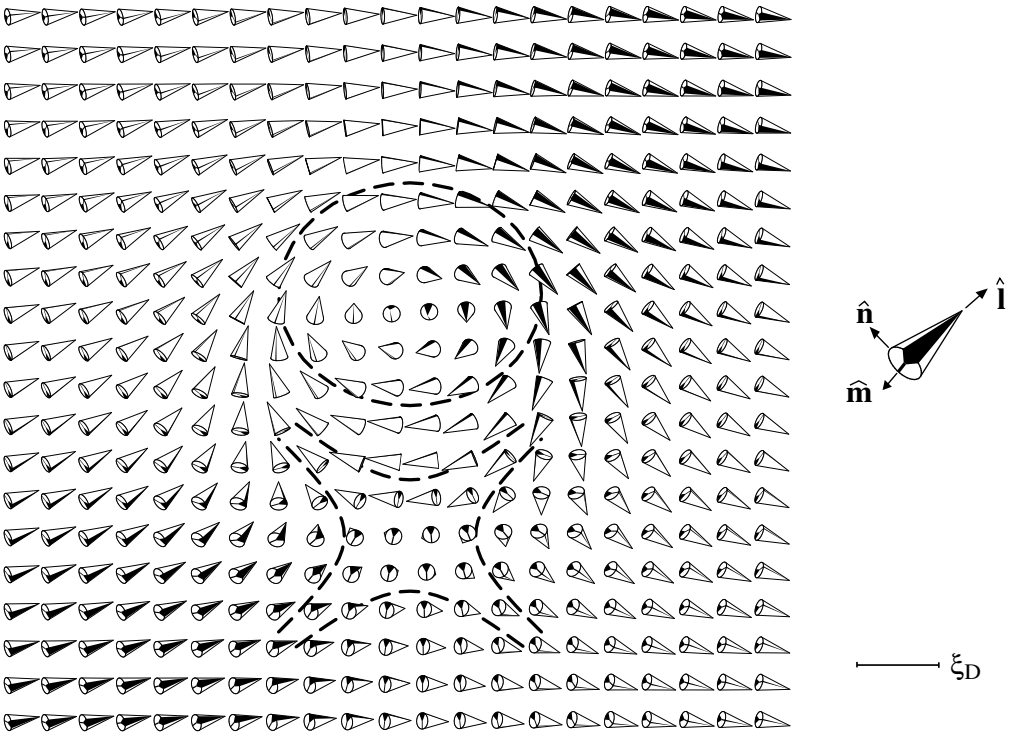

Figure 6: Vortex line with $n = 2$ has a singularity-free order parameter structure and the two circulation quanta of the vortex line correspond to a 4π phase winding around the vortex, which arises from a continuous orientational distribution over 4π of the orbital $\hat{\mathbf{l}}$ field within the vortex.

counterflow $v_n - v_s$ close to the wall at $R_{\rm eff}$ can be written as (see Fig. 3)

$$v_n - v_s = \Omega R_{\rm eff} - \frac{\kappa N}{2\pi R_{\rm eff}}. \tag{31}$$

If the critical velocity is assumed to be constant and the vortices are formed at the distance $R_{\rm eff}$ from the center of the container, then the angular velocity difference $\Delta\Omega$ for vortex events is obtained from Eq. (31). Solving the velocities for N and $N+1$ vortices gives

$$\Delta\Omega = \frac{n\hbar}{2m_3 R_{\rm eff}^2}. \tag{32}$$

Thus the winding number n can be extracted directly from a measurement of the increment $\Delta\Omega$. Here it is remarkable that the mass m_3 is really the bare mass of a ^{3}He atom, despite the fact that the atoms in the liquid are strongly interacting.

Now if $n = 2$ is kept fixed, information on the vortex formation site as a function of rotation velocity Ω can be obtained. The measurements and results are presented in publications [P11] and [P12]. The formation site $R_{\rm eff}$ has to be close to the wall because there the counterflow is fastest, but at the wall there is a boundary condition for $\hat{\mathbf{l}}$, making it locked perpendicular to the wall. Therefore, the results confirm that the vortices in ^{3}He-A are indeed formed in the bulk [55].

Equating the radial dependencies of the normal fluid and superfluid velocities yields for the radius of the vortex cluster

$$R_{\rm cluster} = \sqrt{1 - \frac{\Omega_c}{\Omega}} R, \tag{33}$$

which resembles the dependence of $R_{\rm eff}(\Omega)$. Therefore, the vortex formation site may be considered to be pushed closer to the wall by an expanding vortex cluster.

6 Rotating A-B phase-boundary experiment

In the last chapter of this introduction we here consider how to stabilize the interface between the A and B phases of superfluid ^{3}He. The setup is optimized for vortex detection in the rotating state. The properties of vortices at the phase boundary are deduced from independent NMR measurements in both phases.

6.1 Introduction

The state of the condensate in superfluid ^{3}He is described by a 3×3 complex matrix order parameter. The resulting multitude of phases enables one to study superfluid-superfluid

interfaces. Of the many possible phases of ^{3}He, the A phase with gap nodes and the isotropic B phase are the two major ones in the bulk (see Fig. 1).

The phase transition from the A phase to the B phase is of first order and a well defined interface exist between the phases. The structure of the A-B interface is depicted in Fig. 7. Since the system is described by a single order parameter, the transformation of phases into each other across the interface leads to an excess energy that is here called surface tension. Still there are enough degrees of freedom at the boundary to support vortex lines

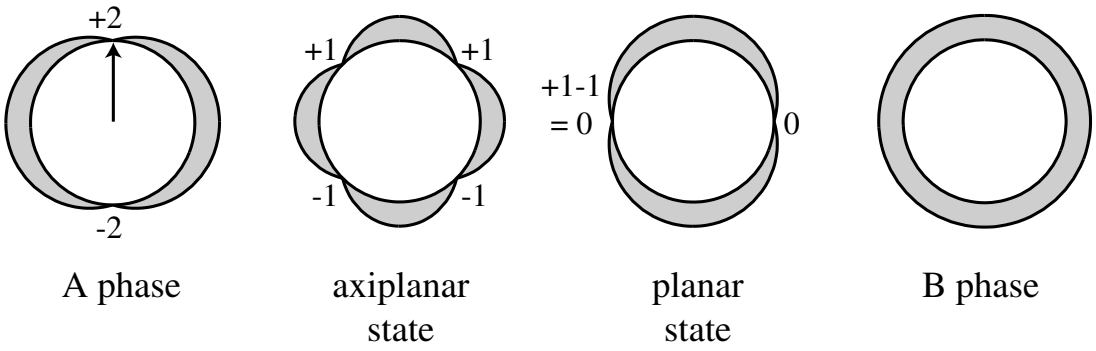

Figure 7: Evolution of the gap nodes in the momentum space at the A-B interface [2]. On the left, the A phase is stable and continuously transforms to the B phase (on the right) through the intermediate axiplanar and planar states. The conserved topological charge is indicated by the numbers in the figure. The surface energy σ_{AB} is a consequence of the additional free energy that arises from the bulk nonequilibrium states and the bending of the order parameter. The width of the boundary is several coherence lengths ($\xi_0 \approx 10\,\mathrm{nm}$).

through the boundary, as has been observed in the case of a moving boundary with the B phase replacing the A phase [56]. The continuation of vortices at the phase boundary is a rather intriguing question. The A phase typically supports doubly quantized continuous $n = 2$ vortices (see Sec. 5) and the B phase singular $n = 1$ vortices. The areas of these vortices differ by a factor of 10^6. According to Ref. [57] vortices should continue through the interface, so one A phase vortex should continue as two B phase vortices.

In principle, all questions that one might ask concerning vortices in a rotating cylinder, can also be extended to the case in the presence of the A-B boundary, like the topological types of defects, their nucleation properties, interactions with each other, and dynamics.

Other physical systems where coherent phase boundaries with intersecting topological defects might become possible include unconventional superconductors and Bose–Einstein

condensates. However, ^{3}He has the advantage that the phases and topological defects are by now well characterized, and methods to distinguish between various defects and to stabilize the A-B boundary exist. Also, the ways to look at defects have advanced to the level that a signal from individual defects can be obtained.

6.2 Earlier experiments on the A-B phase boundary

Despite the obvious interest in the possibility of having an interface of two coherent superfluids, there have not been many experiments conducted on the A-B interface itself.

The interfacial surface energy $\sigma_{\rm AB}$ was measured by Osheroff and Cross [58]. Using NMR, they observed the temperature when the interface passes through a grid of small holes. The knowledge of the value of $\sigma_{\rm AB}$ is of importance when the nucleation properties of the bulk phases are considered.

The velocity of the propagating B phase front in hypercooled A phase was measured in Los Alamos [59]. This was the first experiment to use a high magnetic field to control the hypercooling substantially in the experimental cell. The experiment measured essentially the susceptibility difference of the A and B phases with a SQUID.

A reversible phase transition A↔B in rotating state has been studied in Helsinki [56, 60,61]. A deficit of vorticity after the A→B was observed which depends on the transition time. The velocity of the interface is deduced from the transition time, and it is found that in relatively fast A→B transitions, the A phase vortices are swept to the container walls while in slow transitions part of the vorticity penetrates through the boundary. In slow A→B transitions, some vortices have been identified to be spin-mass vortices [49]. This experiment has a connection to cosmology since it could elucidate the fate of topological defects formed in the early universe [62]. One solution to the monopole problem is that monopoles were swept away by a phase transition front [63, 64]. The monopole problem in short is that attempts to unify the fundamental forces of nature predict the existence of far too many magnetic monopoles in a cosmological context.

At Lancaster University, in the limit of low temperatures and low pressures, the A phase has been stabilized to a region of high magnetic field of $H_{AB} = 340$ mT or greater. With a vibrating wire in the B phase region, information of the gap structure of the B-A interface has been retrieved by observing the Andreev reflection of quasiparticles [65]. The gap nodes of the A phase have been inferred from the measurements of latent heat [66], as well as properties of the nucleation of the superfluid phases have been studied [67, 68].

In none of these experiments, information was retrieved from both phases simultane-

ously. This and the possibility to stabilize the boundary during rotation are the main advancements of the present experiment.

Theoretically, the properties of the phase boundary have been studied in Refs. [57, 58, 69–77]. We note here that a generic numerical calculation on vortices at the phase boundary would be difficult since it should be done in three space dimensions with a 3×3 complex matrix in every point of the grid. Also an adaptive mesh should be used because of the difference of the core sizes of the A and B phase vortices. The length scale for the A phase continuous unlocked vortex is the dipolar length $\xi_D = 10\,\mu$m, and for the B phase singular vortex the length scale is the superfluid coherence length $\xi_0 = 17\,$nm at 2.9 MPa.

6.3 Design considerations

The phase diagram of bulk ^{3}He is a function of pressure, temperature, and magnetic field. A stable A-B phase boundary could be realized to the desired location by applying a gradient of any of these quantities over the sample cell. However, it is not feasible to keep a substantial pressure or temperature gradient for hours, which is the usual time frame of experiments on rotating superfluids.

At first, it seems that the most convenient way to create a stable phase boundary is by arranging the magnetic field so that the A phase is at a higher field than the B phase. Figure 8 shows the phase diagram in the $T - H$ plane at a pressure of 2.9 MPa. However, this is not the optimal field configuration for vortex detection using NMR, as will become obvious below.

Continuous-wave NMR with small tipping angles is so far the most advanced way to probe vortices in ^{3}He. The structure of the vortex lines can be deduced in both the A and B phases [23, 24], and the number of vortex lines can be counted individually as they are nucleated [P11] and [25]. Because the origin of the NMR signals from vortices is different in the A and B phases, the optimal polarization fields for vortex detection are quite different.

6.3.1 Choice of polarization fields for A and B phase NMR

In the A phase, the frequency shifts of small satellite absorption peaks provide the identification of the vortex structure [23], while the amplitude is proportional to the number of the defects. This is because the satellite absorption arises from the excitation of spin waves localized in the soft cores of vortices, and at moderate rotation velocities the soft cores do not overlap.

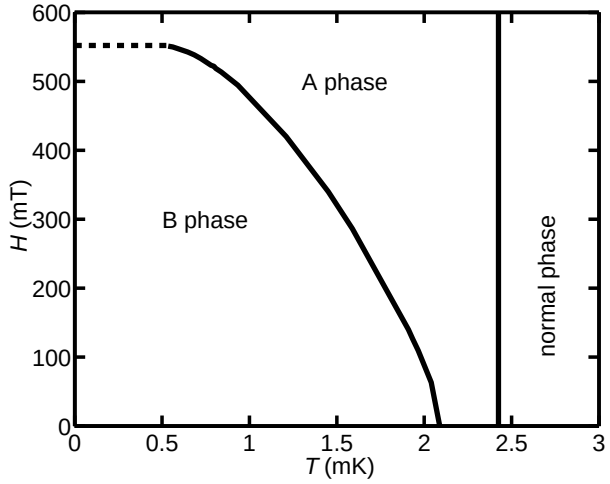

Figure 8: Phase diagram of ^{3}He at 2.9 MPa, constructed from the data given in Ref. [78]. At fixed pressure and temperature, a magnetic-field gradient can be used to stabilize the phase boundary to the desired location in the long cylindrical cell of Fig. 9.

Vortex satellites are shifted away from the main absorption line more and more with increasing pressure and decreasing temperature and magnetic field. Several constraints have to be considered when optimizing these shifts: (1) The magnetic field should be bigger than the dipolar field ($\approx 3\,\mathrm{mT}$), such that in the cores of the topological defects dipolar unlocking occurs giving rise to a satellite in the NMR spectrum. (2) Because the cell is long, and the thermal conductivity of solid helium-3 is low, the pressure should be chosen to be close to the minimum of the melting curve. We choose $p = 2.9\,\mathrm{MPa}$ and $H = 10\,\mathrm{mT}$ although higher pressures would still enhance the supercooling of the A phase, and increase the longitudinal frequency shift.

In the B phase, the nucleation and the number of vortices are identified from the NMR absorption signal envelope, which can be worked out from the local oscillator picture (see [P10]). The increasing normal-superfluid counterflow velocity due to the deficit of vortex lines shifts the NMR absorption from the Larmor frequency to higher frequency. The counterflow affects the global texture in the cell. To change the texture as a function of the counterflow velocity, the radius of the cell should be much bigger than the B phase magnetic coherence length $\xi_H \propto H^{-1}$. The NMR spectra with different ξ_H/R ratios are shown in Ref. [79]. The inner radius of the cell R is chosen to be 3 mm. The considerations for choosing the polarization field $H = \omega/\gamma$ are: (1) The frequency width of the absorption envelope is $\Omega_B^2/2\omega$. At high fields the frequency resolution is lost since

the longitudinal resonance frequency Ω_B is fixed by the spin-orbit interaction and it does not depend on the external field H. Obviously, since the longitudinal resonance frequency is a function of pressure and temperature, the selection of the magnitude of the magnetic field depends on the region of interest in the (p, T) plane. (2) For NMR detection of the changes in the fully developed counterflow peak at $\sin^2\beta = 0.8$, an optimum field exists, which minimizes the line width. The counterflow peak is broadened by the Leggett–Takagi relaxation proportional to H^{-2} and the magnetic field inhomogeneity proportional to H, as considered at low pressures in publication [P10]. Since the frequency range of the Stanford SR560 differential preamplifier does not extend much above 1 MHz, the B phase resonance frequency is chosen so that the corresponding magnetic field is 34 mT.

The structure of the B phase vortex core can be distinguished from the frequency spacing of the spin-wave resonance absorption modes close to Larmor frequency [24]. The minimum observable frequency spacing is limited by the magnetic-field homogeneity, which should obviously be optimized.

From the above considerations, the optimal NMR polarization fields for vortex detection at 2.9 MPa pressure for the A and B phases would be 10 mT and 40 mT, respectively. This contradicts with the idea of stabilizing the phase boundary with a magnetic field gradient (see Fig. 8). Stabilizing the phase boundary to the middle of a long cylinder this way would fix the temperature and lock the experiment to one point in the phase diagram.

Fortunately, the A phase is able to cool at high pressures substantially below the thermodynamical transition point $T_{\rm AB}$. This allows for placing the A phase on the top of the sample cell in low fields, a stable boundary in the middle of the cell, and the B phase in the bottom of the cell at a higher field than the A phase. Two steps are crucial. (1) Smooth walls of the sample container prevent the nucleation of the B phase above $0.5T_c$ as shown in Ref. [80]. Below $0.5T_c$, the lifetime of the A phase is a strong function of temperature, and ionizing radiation as a nucleation mechanism sets in. Quartz as a material for the cylinder wall provides the required smoothness and cleanness. (2) A high magnetic field in the middle of the cell acts as a valve [59], since fields above 550 mT stabilize the A phase over the B phase at all temperatures and pressures. The existing B phase in the lower part of the cell cannot propagate to the top because of this exclusion, and the phase boundary is created. An illustration of the stabilization of the boundary is given in Fig. 9.

With a valve field in the middle of the cell and a smooth-walled container, optimal NMR fields for vortex detection and a stable phase boundary can be simultaneously ob-

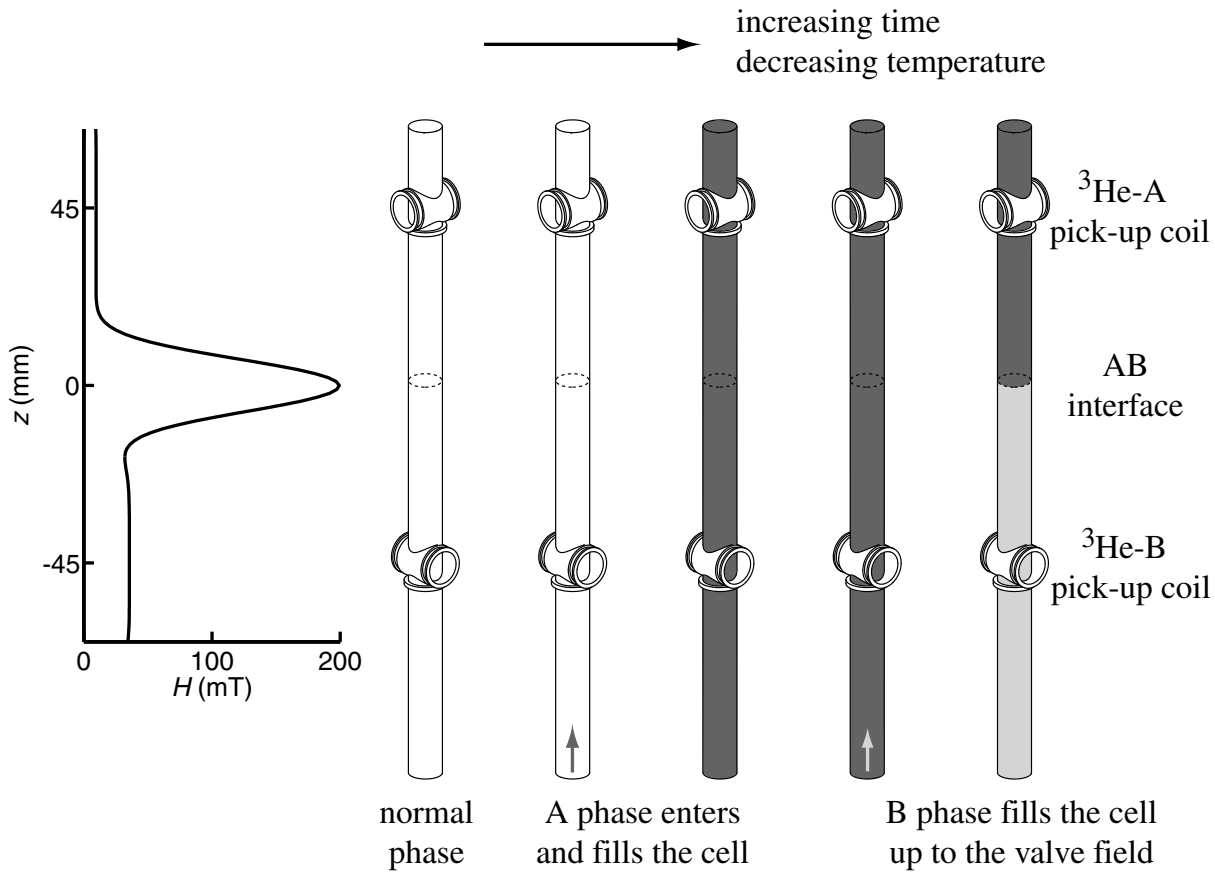

Figure 9: Experimental scheme to stabilize the A-B phase boundary to the middle of a long cylinder. The temperature is lowered in the figure from left to right. The nuclear cooling stage is below the cell. Hence the superfluid phases enter the cell from below. The surface roughness of the platinum-silver sinter below the sample tube nucleates the B phase at a temperature somewhat below $T_{\rm AB}(H = 0\,{\rm mT})$. The B phase then expands up to the valve field region in the middle of the cell, and a stable phase boundary is formed, which can be cooled to temperatures well below $T_{\rm AB}(H = 10\,{\rm mT})$.

tained. An arrangement like this requires a longer cell than those usually used. Such a long cell has a long thermal time constant and thermal gradients are present in the cell during the demagnetization of the nuclear stage. A small orifice $\phi 1$ mm in the bottom of the cell prevents the leakage of vortices into the container from outside where they are nucleated in the rough sinter. A numerical simulation which takes into account the temperature dependencies of the heat capacity and the heat conductivity of normal ^{3}He [81] shows that the time needed to cool down a 150 mm long 6 mm diameter cell from 1 K to below 100 mK is on the order of ten days when the dilution refrigerator keeps the temperature of the nuclear stage at 20 mK. From a precool temperature of 20 mK, it takes around ten hours to reach superfluidity in the cell. In order to diagnose these kinds of problems of cooling the sample ^{3}He, the use of thermometry other than the frequency shift of superfluid ^{3}He is of utmost importance. The thermometers in the experimental setup are briefly discussed in Sec. 6.3.4.

6.3.2 Design of the NMR magnets

The NMR magnet system for the experiment has three coils which are energized from separate power supplies. There are two polarization magnets for NMR, one for the A phase and one for the B phase. One of the magnets produces the valve field that keeps the A-B interface in the middle of the long cylinder.

The polarizing NMR magnets have two main requirements: (1) The field should be as homogeneous as possible over the region of the pick-up coils. (2) The field should not affect the polarization field of the other spectrometer either in magnitude or in homogeneity.

The length of the polarization coils is limited by the available space for the magnet system in the experimental space of the cryostat. Once the length of the polarizing solenoid is fixed, there are two approaches to maximize the homogeneity. One approach is to maximize the coil length/diameter ratio, as then the sample sees the solenoid as an infinitely long solenoid. A lower limit for the diameter of the polarization coils is set by the dimensions of the pickup coils. The other approach is to minimize the coil length/diameter ratio, as then the sample sees the coil as a circular loop and at small distances from the plane of the loop compared to the loop radius the magnetic field does not change rapidly.

We choose the first approach since the second approach makes the second requirement of interference between polarization fields harder to fulfill. With small diameter end compensated NMR solenoids this is easily accomplished with a couple of turns wound in

the reverse direction as shown in Fig. 10.

A superconducting niobium shield around the magnets makes the field profiles less sensitive to machining errors of the coil formers, and also reduces magnetic interference from other devices on the nuclear stage.

The valve magnet should produce a large field at a reasonable current in the middle of the cell without driving the niobium shield into normal state. Therefore the inner diameter of the valve-field coil former, 14 mm, was made as small as reasonably possible. The valve magnet has counterwound compensation coils to minimize the effect on the homogeneity of the two NMR polarization fields. Figure 10 shows the disassembled magnet system with the three concentric inserts.

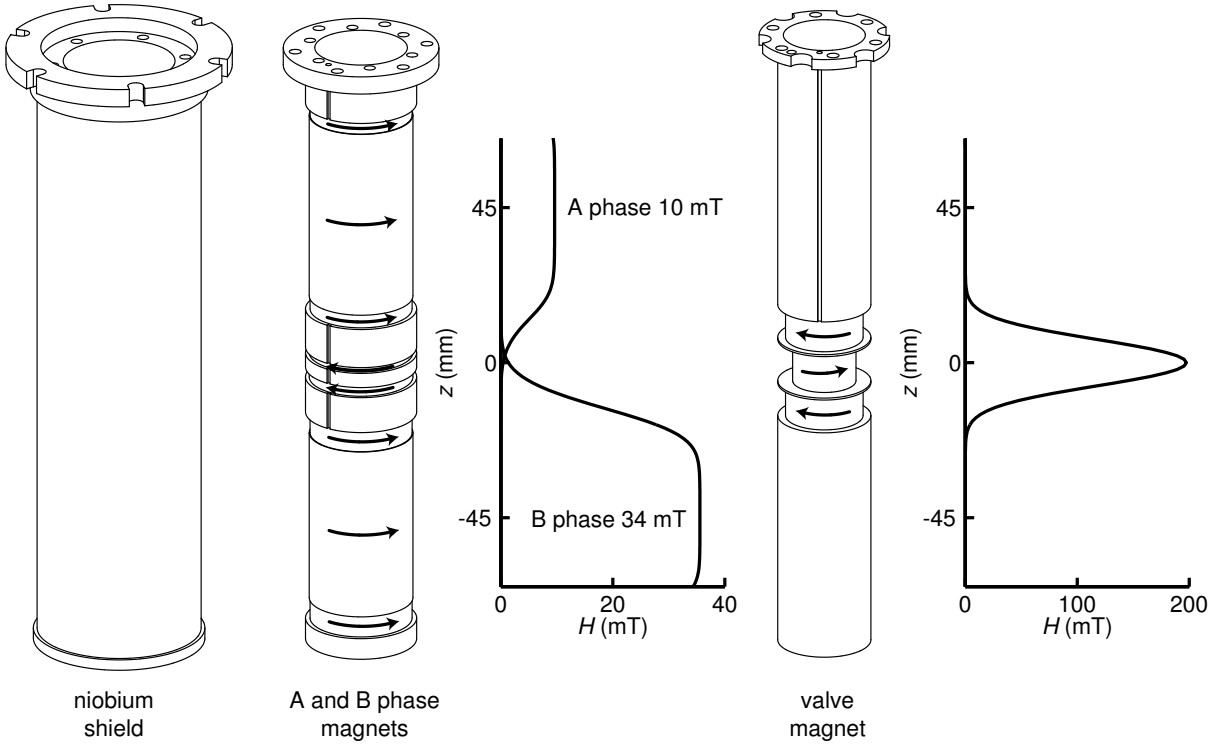

Figure 10: Magnetic field configuration of the experimental setup. The polarization fields for the A and B phases as well as the valve field at the A-B phase boundary are independent from each other. The arrows show the direction of the windings. Two heat-treated copper cylinders are inserted inside the brazen valve-magnet bobbin in order to reduce the radiative losses of the NMR tank circuit.

The polarization magnets were designed by optimizing ratios characterizing the field homogeneity of the A and B phase spectrometers numerically. The ratio for the A phase

magnet is given by

$$\frac{\sqrt{\langle H_A^2\rangle_A - \langle H_A\rangle_A^2} + \sqrt{\langle H_A^2\rangle_B - \langle H_A\rangle_B^2}}{\langle H_A\rangle_A}, \tag{34}$$

where H_A is the magnetic field produced by the A phase polarization coil and the $\langle\rangle_B$ denotes that the average is calculated over the region of the B phase pick-up coil. Incidentally, the average magnetic field of the A phase magnet is zero at the B phase pick-up coil region, and vice versa. The same applies to the valve magnet. Fields produced by the A phase, B phase, and the valve-field coils are independent of each other, as seen in Fig. 11. The polarization fields change the magnitude of the maximum of the valve field by 1 mT at most.

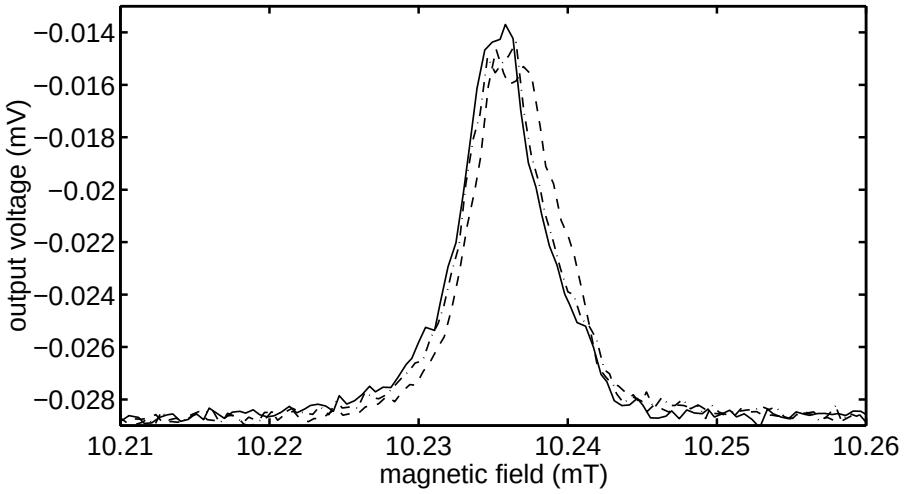

Figure 11: Spectra of normal phase ^{3}He signal measured with the upper spectrometer. The solid line is with only the A phase magnet energized. In the dashdotted line 2.1 A current is fed to the B phase magnet giving a field of 40 mT. In the dashed line all magnets are used with 1.5 A to the valve magnet giving a field of 130 mT. The interference on the A phase spectrometer NMR linewidth from other magnets of the setup is tolerable. The output voltage measured with the lock-in amplifier is shown. The Q value of the spectrometer is 11600.

The shape of the phase boundary at $\Omega = 0$ rad/s is determined by the shape of the constant-field contours of the valve field. Shapes of the boundary at different currents of the valve magnet are shown in Fig. 12. It is seen that the position of A-B boundary is not a strong function of the applied current. A 100 mA increase in current can cause a change in the position of the boundary of 1 mm at most. This means that a strong modulation of the boundary position with a changing applied current to the valve magnet is not feasible

with this setup.

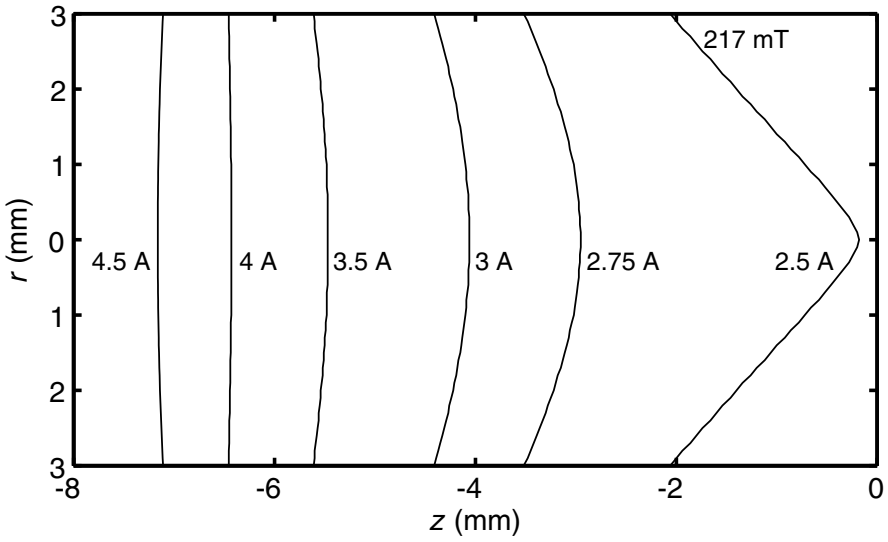

Figure 12: Profiles of the A-B phase boundary at $\Omega = 0\,\mathrm{rad/s}$ calculated numerically from the constant-field contours of 217 mT produced by the valve magnet at different applied currents. The center of the valve magnet is at $z = 0\,\mathrm{mm}$. The boundary is flat when it is 6.5 mm below the center and the value of the field is 1.6 times the field needed to stabilize the boundary. At 2.9 MPa a magnetic field of 217 mT is enough to stabilize the boundary from the temperature of $0.72T_c$ up to $T_{\mathrm{AB}} = 0.86T_c$.

6.3.3 NMR pick-up coils

The geometry of the pick-up coils used in the spectrometer is a coaxial pair of coils. The average spacing of the halves is 10 mm and the diameter of the windings is 9 mm. The windings have 54+54 turns in two layers giving an inductance of $L = 24\,\mu\mathrm{H}$. The A-phase spectrometer has a fixed frequency of $f_0 = 332\,\mathrm{kHz}$ and a quality factor of $Q = 10\,000$. The B-phase tank circuit has $f_0 = 1.32\,\mathrm{MHz}$ and $Q = 7\,500$. The resonance frequencies correspond to magnetic fields of 10.2 mT and 40.7 mT, respectively, since $\gamma/(2\pi) = 32.436\,\mathrm{kHz/mT}$ for ^{3}He. The pick-up coils are wound from 50 μm multifilament NbTi wire and the layers are fixed with diluted varnish. A small hydrogen contribution is observed to give a tilted background despite the fact that the gyromagnetic ratios of hydrogen (^{1}H) and helium (^{3}He) differ by a factor of 1.31. Single filament niobium wire with a diameter of 25 μm was found not to be strong enough in consecutive cooldowns when wound on a quartz former, but has the advantage of a negligible hydrogen background.

Comparison of the integrated area of the absorption signal in the normal phase to the static susceptibility gives a value of two percent for the filling factor ξ (see Sec. 2.2.1). The filling factor is optimized by placing the pick-up coils close to the sample. This compromises the homogeneity of the RF excitation field produced by the pick-up coil. On the average the signal picked up from the wall of the container is 20% stronger that the signal picked up from the center of the container. More than 90% of the signal strength comes from the region less than 6 mm in the axial direction from the center of the pick-up coils.

6.3.4 Thermometers

The experimental setup adds two thermometers, a melting-curve thermometer and a pulsed platinum NMR thermometer, on the nuclear stage that were not used in the published articles [P1–P12].

The melting curve thermometer is based on a Straty–Adams type capacitive pressure gauge. The capacitive pressure gauge has a resolution of 40 pF/MPa at 3.4 MPa. It is insensitive to the rotation of the cryostat up to the maximum speed of 3.5 rad/s.

During the experiments in addition to the frequency shifts of the A and B phase NMR signals, pulsed NMR on ^{195}Pt nuclei is available for thermometry. Slow demagnetization with the HVL10 power supply (see Fig. 13) allows one to stabilize the temperature of the nuclear stage within 1 μK. The pulsed platinum NMR thermometer operating at 125 kHz works well from 40 mK down following the temperature of the nuclear stage. It is calibrated against the melting curve thermometer.

6.3.5 Instrumentation

Most instruments on the rotating platform have to be computer interfaced with the GPIB bus making them controllable during the rotating measurements. Figure 13 shows the schematic diagram of the NMR data acquisition setup.

The data acquisition programs are written in C and Tcl/Tk languages. Tcl/Tk bindings to the GPIB library allow rapid prototyping and program development. The measurement computer is running the Linux operating system.

6.4 Possible experiments

The described setup is the first investigating the stable A-B phase boundary in rotation. The vortices at the phase boundary will be inferred indirectly from CW-NMR measure-

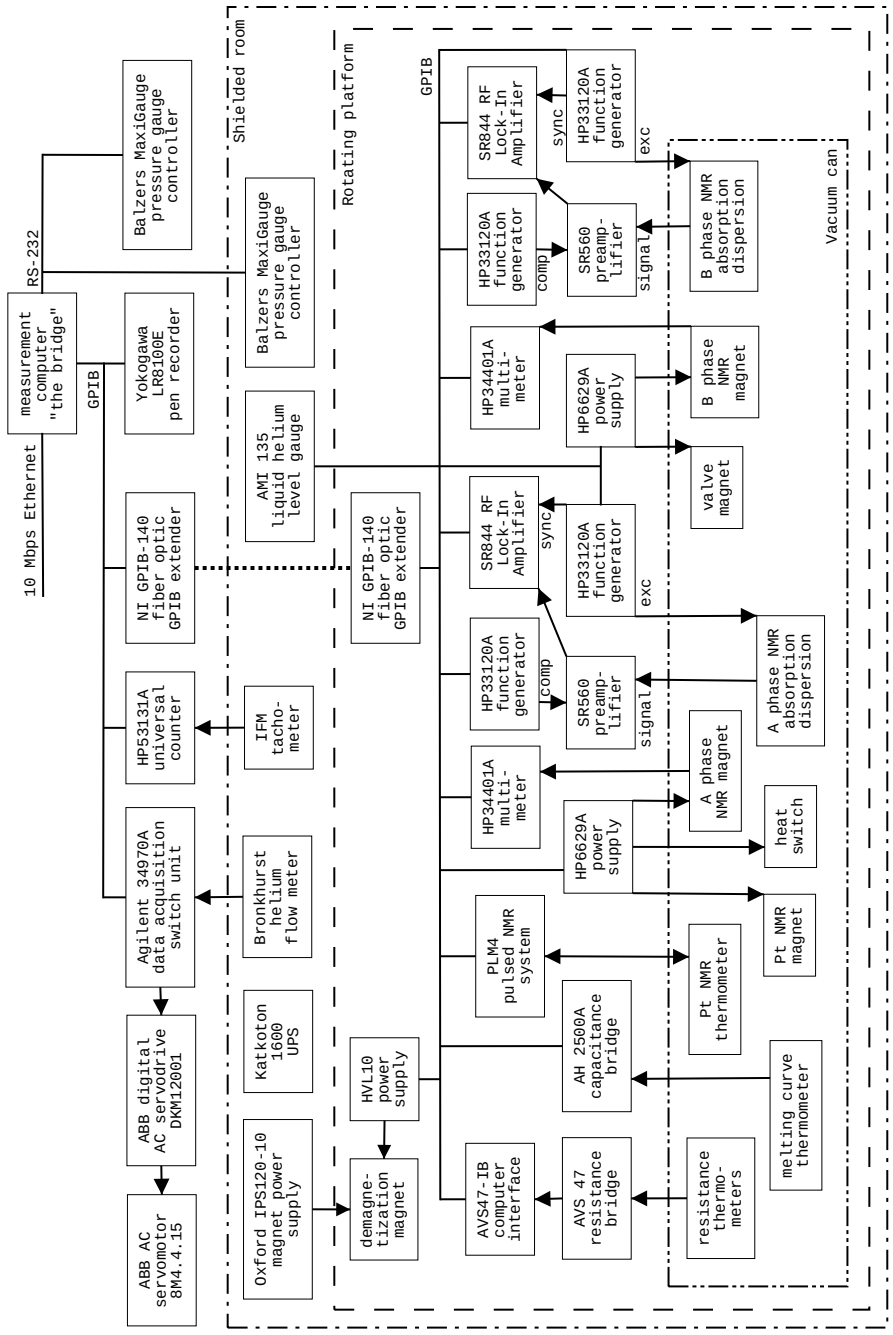

Figure 13: Instrumentation of the Rota I cryostat for the A-B phase-boundary experiment. Items inside the vacuum can are homemade, while other components in the setup are commercial with the exception of HVL10 [82].

ments in A and B phases far away from the boundary. Retrieving direct NMR response from the boundary would be desirable, since monopoles and half quantum vortices have been predicted to exist [72], but they have not been experimentally observed in other ^{3}He experiments. This would require a new approach since in the present case the valve field is not homogeneous and a high Q resonator works at a fixed frequency that cannot be changed from room temperature.

The basic experiment is to establish the phase boundary in the cell and to ramp the rotation velocity in a linear fashion. The continuous vortices in the A phase have lower critical velocity than the vortices in the B phase [36, 55]. The formation of the A-phase vortices is observed with the A-phase spectrometer. Whether the doubly quantized A-phase vortices cross the boundary and transform into singly quantized B-phase vortices can be detected from the change in the B phase NMR signal. One possibility is that the A phase vortices do not cross the A-B phase boundary but bend to the wall at the interface. Slow A→B transitions suggest a critical vortex density on the A-B interface of A-phase vortices [56]. At higher density the vortices penetrate the interface collectively.

The magnetic field configuration in the long cell makes other interesting measurements possible with no or slight changes in the experimental setup.

In the A phase there are many different types of quantized vorticity which can be classified with topological invariants. One of them is ν_d defined as

$$\nu_d = \frac{1}{4\pi} \int \hat{\mathbf{d}} \cdot \frac{\partial \hat{\mathbf{d}}}{\partial x} \times \frac{\partial \hat{\mathbf{d}}}{\partial y} \, dx \, dy. \tag{35}$$

The prominent vortex type at high fields is the continuous unlocked vortex having $\nu_d = 0$ described in Sec. 5. At low fields the orbital anisotropy axis $\hat{\mathbf{l}}$ and the magnetic anisotropy vector $\hat{\mathbf{d}}$ are locked $\hat{\mathbf{d}} = \pm\hat{\mathbf{l}}$ and the low field vortices have $\nu_d = 1$ or $\nu_d = 2$ [52]. A topological first-order transition from a continuous locked vortex formed in a low magnetic field to a continuous unlocked vortex upon increasing the field past the upper critical field $H_{c1} = 4\,\mathrm{mT}$ has been observed [83]. However, in a supercooled A phase the continuous locked vortices have been observed to exist at least up to magnetic fields of 12 mT [23]. This metastability makes two different experiments possible.

Consider the whole long cylinder filled with only A phase. Once in the supercooled state, set a 10 mT NMR field in the upper spectrometer and zero field in the lower NMR spectrometer. Then in the spinup of the container, continuous locked vortices should be formed in the lower part of the cell because they have a lower critical velocity than continuous unlocked vortices. These vortices will expand to the upper spectrometer region and are to be observed individually as they are nucleated. The critical velocity

and hopefully the quantization can be determined. For the quantization there are two possibilities, $n = 2$ or $n = 4$, according to Ref. [52].

With the valve magnetic field up to 400 mT, the magnetic field triggering the transition from continuous locked vortices to continuous unlocked vortices can be measured accurately as a function of temperature, as it happens. This would shed light on the nature of the topological transition. One possibility is the creation of a point defect in the $\hat{\mathbf{d}}$ field called hedgehog. This hedgehog would move along the vortex core axis and wipe out the charge ν_d [84]. Whether such monopoles can be detected during the transition by NMR is an interesting open question.

The measurement of the Kapitza resistance across the phase boundary has been theoretically considered by Yip [70]. There might be a possibility for the measurement of the boundary resistance since the frequency shift of the NMR provides an accurate intrinsic thermometer in the A phase and high RF excitation can be used to heat the sample.

Repeating the measurements of Parts *et al.* [56] might become worthwhile since after those measurements, methods to create the vortex sheet [85] and singular vortex lines have been found. By carefully preparing the vortex state in the A phase one might find out the details on what happens to different vortices in a A→B transition as a function of the transition time.

7 List of publications

This thesis is based on the following peer reviewed original publications.

[P1] Y. Kondo, J. H. Koivuniemi, J. J. Ruohio, V. M. Ruutu, and M. Krusius, "Optimization of high-Q low frequency NMR measurement," *Czech. J. Phys.*, vol. 46-Suppl., pp. 2843–2844, 1996.

In NMR spectrometers utilizing a high Q tank circuit, radiative losses to low conducting magnet formers were found to be a possible limiting factor for an even higher Q value. A workaround for this problem was developed.

[P2] Ü. Parts, V. V. Avilov, J. H. Koivuniemi, M. Krusius, J. J. Ruohio, and V. M. H. Ruutu, "Vortex arrays of coexisting singly and doubly quantized vortex lines in ^{3}He-A," *Czech. J. Phys.*, vol. 46-Suppl., pp. 13–14, 1996.

[P3] Ü. Parts, V. V. Avilov, N. B. Kopnin, M. Krusius, J. J. Ruohio, and V. M. H. Ruutu, "Coexistence of single and double quantum vortex lines," *Phys. Rev. B*, vol. 62, pp. 5865–5876, Sept. 2000.

We have shown that in superfluid ^{3}He-A topologically stable vortex lines with different quantization can appear simultaneously. Two different methods to prepare states with coexisting singly and doubly quantized vortices were found. The radial compositions of such states were compared to numerical simulations, and one of the procedures was identified to lead into the minimum energy configuration.

[P4] V. M. Ruutu, J. J. Ruohio, M. Krusius, B. Plaçais, E. B. Sonin, E. V. Thuneberg, and Wen Xu, "Annihilation of quantized vortex lines in rotating ^{3}He-A," *Czech. J. Phys.*, vol. 46-Suppl., pp. 9–10, 1996.

[P5] V. M. Ruutu, J. J. Ruohio, M. Krusius, B. Plaçais, E. B. Sonin, and W. Xu, "Annihilation of vortex lines in rotating superfluid ^{3}He," *Phys. Rev. B*, vol. 56, pp. 14089–14092, Dec. 1997.

[P6] V. M. Ruutu, J. J. Ruohio, M. Krusius, B. Plaçais, and E. B. Sonin, "Metastability in decelerating rotation of superfluid ^{3}He-B," *Physica B*, vol. 255, pp. 27–40, 1998.

We have performed the first quantitative measurements on vortex annihilation in the rotating ^{3}He superfluids. At the destabilizing velocity, the vortices are lost to the lateral walls where they annihilate, at most in bunches of a few lines. In the

B phase, at a low rotation velocity the number of B phase singular vortices was found to exceed the equilibrium number in decelerating rotation. The destabilizing velocity of an vortex array in a two-dimensional framework was numerically studied in Sec. 3.2.

[P7] V. B. Eltsov, V. V. Dmitriev, M. Krusius, J. J. Ruohio, and G. E. Volovik, "New modes of stable spin precession in superfluid ^{3}He-B," *J. Low Temp. Phys.*, vol. 113, pp. 645–650, Dec. 1998.

[P8] V. V. Dmitriev, V. B. Eltsov, M. Krusius, J. J. Ruohio, and G. E. Volovik, "Superflow-stabilized nonlinear NMR in rotating ^{3}He-B," *Phys. Rev. B*, vol. 59, pp. 165–168, Jan. 1999.

Exotic spin precession modes exist in the B phase exhibiting nonlinear NMR response. The magnitude of the magnetization of some of stable modes can differ from the equilibrium value. The sensitivity of such states to the number of vortices and to the counterflow between the superfluid and normal fluid fraction was investigated. Once created near T_c, some modes were found to be stable upon cooling down to $0.8T_c$, and their stability regimes were found to be more extended at a field of 21 mT than in the previous experiments at 10 mT, but the modes were found not to be feasible for vortex studies.

A new nonlinear NMR response was observed to develop as the counterflow was increased at a high RF excitation level. In this new mode of spin precession, the orbital angular momentum $\mathbf{L}$ is oriented along the flow direction transverse to the external magnetic field. The nature of this mode was identified by comparing the NMR response to the numerical solutions of the Leggett-Takagi spin-dynamic equations.

[P9] R. Schanen, R. Blaauwgeers, V. B. Eltsov, M. Krusius, and J. J. Ruohio, "NMR measurement of quantized vortex lines in rotating ^{3}He-B," *Physica B*, vol. 284-288, pp. 254–255, July 2000.

[P10] J. Kopu, R. Schanen, R. Blaauwgeers, V. B. Eltsov, M. Krusius, J. J. Ruohio, and E. V. Thuneberg, "NMR line shape of rotating ^{3}He-B at large counterflow velocity," *J. Low Temp. Phys.*, vol. 120, pp. 213–232, Aug. 2000.

Single-vortex sensitivity, or vortex line counting, in the B phase has proven to be a useful tool in the study of vortices nucleated by neutron irradiation [25]. In

order to extend this experiment to lower temperatures, the sensitivity of NMR for vortex detection as a function of magnetic field was studied. Experimental NMR line shapes were compared to curves obtained from a numerical model taking into account different line broadening mechanisms.

[P11] R. Blaauwgeers, V. B. Eltsov, M. Krusius, J. J. Ruohio, R. Schanen, and G. E. Volovik, "Double-quantum vortex in superfluid ^{3}He-A," *Nature*, vol. 404, pp. 471–473, Mar. 2000.

[P12] R. Blaauwgeers, V. B. Eltsov, M. Krusius, J. J. Ruohio, and R. Schanen, "NMR measurement of quantized vortex lines in rotating ^{3}He-A," *Physica B*, vol. 284-288, pp. 250–251, July 2000.

We have measured the NMR response of the dipole-unlocked vortex in the A phase with improved resolution. The circulation of this vortex structure was found to be two circulation quanta. This is the first time that the circulation of a doubly-quantized vortex was determined directly in any quantum fluid. This confirms the working hypothesis that doubly-quantized vortices indeed are the prominent form of vorticity in the A phase.

At the sensitivity of a single vortex event, it was possible to analyze the position of the vortex formation site as a a function of rotation velocity by using correlation analysis on the measurement data.

7.1 Author's own contribution

The research work presented in this thesis is a result of team work.

I am responsible for the work on identifying losses in the high-Q LC resonator presented in [P1]. I designed the experimental cell and the pickup-coil setup that was used in [P9]–[P12].

I took care of the cryostat maintenance since the beginning of 1996, and I was responsible for the data acquisition and instrumentation starting from [P4]. The recording of the dispersion of the NMR signal was added in the end of 1994, which is necessary for correcting the NMR signal in a high Q setup. The whole data acquisition system including the software part was completely revamped in the beginning of 1996.

I did part of the data analysis in [P2], [P3], and [P7]–[P11]. Part of the measurements in [P4]–[P10] were done by me. Also, I participated in the writing process of the published papers by reading and commenting the versions at their different stages.

I played an active role in the design and in the construction of the A-B phase-boundary experiment described in the latter part of this introduction, as well as the planning of the possible experiments in this setup. At the time of writing this, January 2001, the experiment has yet to produce the first results. The idea of placing the A phase into a lower field than the B phase, using a compensated axial valve magnet instead of a transversal magnet, and the numerical design of the whole magnet system are altogether due to the author. [Note added: The phase boundary in the rotating state was successfully stabilized for the first time on 23rd of February, 2001.]

7.2 Other related publications

Other publications by the author not included in this thesis.

[P13] V. B. Eltsov, R. Blaauwgeers, M. Krusius, J. J. Ruohio, and R. Schanen, "Dynamic response of the equilibrium vortex sheet in rotating ^{3}He-A," *Physica B*, vol. 284-288, pp. 252–253, July 2000.

[P14] K.-U. Taubenreuther, R. Schuhmann, E. Nazaretski, L. Hristakos, H. Götz, G. Eska, and J. Ruohio, "Pulsed NMR investigations on normal-fluid ^{3}He in restricted geometries," *Physica B*, vol. 284-288, pp. 295–296, July 2000.

[P15] R. Blaauwgeers, V. B. Eltsov, M. Krusius, J. Ruohio, and R. Schanen, "Quantized vorticity in superfluid ^{3}He-A: Structure and dynamics," in *Superfluid Turbulence and Quantized Vortex Dynamics* (C. F. Barenghi, ed.), (Berlin), Springer Verlag, 2001.

Acknowledgments

The work done in the ROTA-group is a team effort. I am obliged to Matti Krusius as the group leader for giving me the opportunity to work under his supervision. I owe much to my coworkers for learning new and old things about experimental low temperature physics: Yasushi Kondo, Ville Ruutu, Wen Xu, Roch Schanen, Rob Blaauwgeers, Volodya Eltsov, Jaakko Koivuniemi, Ülo Parts, Bernard Plaçais, Vladimir Dmitriev, Sergei Boldarev, and Antti Finne.

This work would have been impossible without the theoretical support by Viatcheslav Avilov, Nikolai Kopnin, Edouard Sonin, Erkki Thuneberg, Juha Kopu, and Grisha Volovik.

I thank people in the other research groups for help and discussions, including Harry Alles, Alosha Babkin, Jussi Ruutu, Jari Saramäki, Giggs Tvalashvili, and Viktor Tsepelin from the Interface-group, Janne Viljas, Risto Hänninen, and Kaa-Ke Schakel from the Theory group, Kaj Nummila, Juha Tuoriniemi, Tauno Knuuttila, Juha Martikainen, and Weijun Yao from the YKI-group, and Pertti Hakonen, Jari Penttilä, and Leif Roschier from the Nano-group.

I am obliged to Arvi Isomäki and Antero Salminen at the liquefier for providing liquid nitrogen and helium, and to the people, especially Markku Korhonen, in the workshop for machining various pieces for the experimental setups. The Director of the laboratory, Mikko Paalanen, and other people in the lab administration are thanked for help with practical matters.

I gratefully acknowledge scholarships from the Helsinki University of Technology, Research Foundation of Helsinki University of Technology, and Vilho, Kalle, and Yrjö Väisälä Foundation, as well as funding from National Graduate School in Materials Physics.

Finally, I am indebted to my parents and my brother for all possible support during these years. Eve deserves a lot of hugs and kisses.

Otaniemi, January 2001

Jaakko Ruohio

References

[1] D. Vollhardt and P. Wölfle, *The Superfluid Phases of Helium 3*. London / New York / Philadelphia: Taylor & Francis, 1990.

[2] G. E. Volovik, *Exotic Properties of Superfluid ^3He*, vol. 1 of *Series in Modern Condensed Matter Physics*. Singapore: World Scientific, 1992.

[3] O. V. Lounasmaa and E. Thuneberg, "Vortices in rotating superfluid ^{3}He," in *Proc. Natl. Acad. Sci. USA*, vol. 96, pp. 7760–7767, July 1999.

[4] E. B. Sonin, "Vortex oscillations and hydrodynamics of rotating superfluids," *Rev. Mod. Phys.*, vol. 59, no. 1, pp. 87–155, 1987.

[5] P. J. Hakonen, O. T. Ikkala, S. T. Islander, T. K. Markkula, P. Roubeau, K. M. Saloheimo, D. I. Garibashvili, and J. S. Tsakadze, "Rotating minilab - design and performance," *Physica B*, vol. 107, pp. 567–568, 1981.

[6] B. C. Crooker, B. Hebral, and J. D. Reppy, "Critical velocity in superfluid ^{3}He-B," *Physica B*, vol. 108, no. 1–3, pp. 795–796, 1981.

[7] R. H. Salmelin, J. M. Kyynäräinen, M. P. Berglund, and J. P. Pekola, "A cryopump-operated rotating nuclear demagnetization cryostat for research on superfluid ^{3}He," *J. Low Temp. Phys.*, vol. 76, no. 1/2, pp. 83–106, 1989.

[8] J. D. Close, R. J. Zieve, and R. E. Packard, "Continuously pumped rotating millikelvin cryostat," *Physica B*, vol. 165&166, pp. 57–58, Aug. 1990.

[9] H. E. Hall, J. R. Hook, S. Wang, A. J. Armstrong, and T. D. Bevan, "Rotating millikelvin cryostat," *Physica B*, vol. 194–196, pp. 41–42, Feb. 1994.

[10] O. Avenel and E. Varoquaux, "Josephson effect and quantum phase slippage in superfluids," *Phys. Rev. Lett.*, vol. 60, pp. 416–419, Feb. 1988.

[11] C. Bäuerle, Yu. M. Bunkov, S. N. Fisher, H. Godfrin, and G. R. Pickett, "Laboratory simulation of cosmic string formation in the early universe using superfluid ^{3}He," *Nature*, vol. 382, pp. 332–334, July 1996.

[12] D. I. Bradley, "Repetitive single vortex-loop creation by a vibrating wire in superfluid ^{3}He-B," *Phys. Rev. Lett.*, vol. 84, pp. 1252–1255, Feb. 2000.

[13] D. D. Osheroff, R. C. Richardson, and D. M. Lee, "Evidence for a new phase of solid He^3," *Phys. Rev. Lett.*, vol. 28, pp. 885–888, Apr. 1972.

[14] M. H. Anderson, J. R. Ensher, M. R. Matthews, C. E. Wieman, and E. A. Cornell, "Observation of Bose–Einstein condensation in a dilute atomic vapor," *Science*, vol. 269, pp. 198–201, July 1995.

[15] M. R. Matthews, B. P. Anderson, P. C. Haljan, D. S. Hall, C. E. Wieman, and E. A. Cornell, "Vortices in a Bose–Einstein condensate," *Phys. Rev. Lett.*, vol. 83, pp. 2498–2501, Sept. 1999.

[16] K. W. Madison, F. Chevy, W. Wohlleben, and J. Dalidard, "Vortex formation in a stirred Bose–Einstein condensate," *Phys. Rev. Lett.*, vol. 84, pp. 806–809, Jan. 2000.

[17] G. E. Volovik, "Field theory in superfluid ^{3}He: What are the lessons for particle physics, gravity, and high-temperature superconductivity?," in *Proc. Natl. Acad. Sci. USA*, vol. 96, pp. 6042–6047, May 1999.

[18] O. Avenel, P. Hakonen, and E. Varoquaux, "Detection of the rotation of the earth with a superfluid gyrometer," *Phys. Rev. Lett.*, vol. 78, pp. 3602–3605, May 1997.

[19] S. V. Pereverzev, A. Loshak, S. Backhaus, J. C. Davis, and R. E. Packard, "Quantum oscillations between two weakly coupled reservoirs of superfluid ^{3}He," *Nature*, vol. 388, pp. 449–451, July 1997.

[20] S. Backhaus, S. V. Pereverzev, A. Loshak, J. C. Davis, and R. E. Packard, "Direct measurement of the current-phase relation of a superfluid ^{3}He-B weak link," *Science*, vol. 278, pp. 1435–1438, Nov. 1997.

[21] D. I. Bradley, Yu. M. Bunkov, D. J. Cousins, M. P. Enrico, S. N. Fisher, M. R. Follows, A. M. Guénault, W. M. Hayes, G. R. Pickett, and T. Sloan", "Potential dark matter detector? The detection of low energy neutrons by superfluid ^{3}He," *Phys. Rev. Lett.*, vol. 75, pp. 1887–1890, Sept. 1995.

[22] C. P. Slichter, *Principles of Magnetic Resonance*, vol. 1 of *Springer Series in Solid-State Sciences*. Berlin / Heidelberg / New York: Springer-Verlag, second revised and expanded ed., 1978.

[23] Ü. Parts, J. M. Karimäki, J. H. Koivuniemi, M. Krusius, V. M. H. Ruutu, E. V. Thuneberg, and G. E. Volovik, "Phase diagram of vortices in superfluid ^{3}He-A," *Phys. Rev. Lett.*, vol. 75, pp. 3320–3323, Oct. 1995.

[24] P. J. Hakonen, M. Krusius, M. M. Salomaa, J. T. Simola, Yu. M. Bunkov, V. P. Mineev, and G. E. Volovik, "Magnetic vortices in rotating superfluid ^{3}He-B," *Phys. Rev. Lett.*, vol. 51, pp. 1362–1365, Oct. 1983.

[25] V. M. H. Ruutu, V. B. Eltsov, A. J. Gill, T. W. B. Kibble, M. Krusius, Yu. G. Makhlin, B. Plaçais, G. E. Volovik, and W. Xu, "Vortex formation in neutron-irradiated superfluid ^{3}He as an analogue of cosmological defect formation," *Nature*, vol. 382, pp. 334–336, July 1996.

[26] A. J. Leggett, "The spin dynamics of an anisotropic Fermi superfluid (^{3}He?)," *Ann. Phys.*, vol. 85, pp. 11–55, May 1974.

[27] B. H. Suits, A. N. Garroway, and J. B. Miller, "Super-Q detection of transient magnetic resonance signals," *J. Magn. Reson.*, vol. 132, pp. 54–64, May 1998.

[28] D. Kajfez and P. Guillon, eds., *Dielectric Resonators*. Oxford, Mississippi: Vector Fields, 1990.

[29] V. Ruutu, J. Koivuniemi, Ü. Parts, A. Hirai, and M. Krusius, "High sensitivity NMR measurements at low temperature and frequency," *Physica B*, vol. 194–196, pp. 159–160, Feb. 1994.

[30] J. C. Wheatley, "Experimental properties of superfluid ^{3}He," *Rev. Mod. Phys.*, vol. 47, pp. 415–470, Apr. 1975.

[31] L. J. Campbell and R. M. Ziff, "Vortex patterns and energies in a rotating superfluid," *Phys. Rev. B*, vol. 20, pp. 1886–1902, Sept. 1979.

[32] E. J. Yarmchuk, M. J. V. Gordon, and R. E. Packard, "Observation of stationary vortex arrays in rotating superfluid helium," *Phys. Rev. Lett.*, vol. 43, pp. 214–217, July 1979.

[33] A. J. Manninen, T. D. C. Bevan, J. B. Cook, H. Alles, J. R. Hook, and H. E. Hall, "Vortex mutual friction, orbital inertia, and history-dependent textures in rotating superfluid ^{3}He-A," *Phys. Rev. Lett.*, vol. 77, pp. 5086–5089, Dec. 1996.

[34] W. Xu, B. Plaçais, V. M. Ruutu, and M. Krusius, "Equilibrium number of quantized vortex lines in rotating ^{3}He-B," *Czech. J. Phys.*, vol. 46-Suppl., pp. 11–12, 1996.

[35] V. M. H. Ruutu, Ü. Parts, J. H. Koivuniemi, N. B. Kopnin, and M. Krusius, "Intrinsic and extrinsic mechanisms of vortex formation in superfluid ^{3}He-B," *J. Low Temp. Phys.*, vol. 107, pp. 93–164, Apr. 1997.

[36] Ü. Parts, J. H. Koivuniemi, M. Krusius, V. M. H. Ruutu, and S. R. Zakazov, "Nucleation of single vortex lines in rotating ^{3}He-B," *Physica B*, vol. 194–196, pp. 771–772, 1994.

[37] D. Stauffer and A. L. Fetter, "Distribution of vortices in rotating helium II," *Phys. Rev.*, vol. 168, pp. 156–159, Apr. 1968.

[38] L. J. Campbell, "Transverse normal modes of finite vortex arrays," *Phys. Rev. A*, vol. 24, pp. 514–534, July 1981.

[39] T. H. Havelock, "The stability of motion of rectilinear vortices in ring formation," *Phil. Mag.*, vol. 11, pp. 617–633, Feb. 1931.

[40] P. Mathieu, J. C. Marechal, and Y. Simon, "Spatial distribution of vortices and metastable states in rotating He II," *Phys. Rev. B*, vol. 22, pp. 4293–4306, Nov. 1980.

[41] M. Krusius, J. S. Korhonen, Y. Kondo, and E. B. Sonin, "Collective motion of quantized lines in rotating superfluid ^{3}He-B," *Phys. Rev. B*, vol. 47, pp. 15113–15143, June 1993.

[42] R. J. Donnelly, *Quantized Vortices in Helium II.* Cambridge: Cambridge University Press, 1991.

[43] L. J. Campbell, "Rotational speedups accompanying angular deceleration of a superfluid," *Phys. Rev. Lett.*, vol. 43, pp. 1336–1339, Oct. 1979.

[44] W. F. Brinkman and H. Smith, "Large angle tipping frequency shifts in pulsed NMR for ^{3}He(B)," *Phys. Lett.*, vol. 53A, pp. 43–44, May 1975.

[45] E. V. Thuneberg, "Hydrostatic theory of superfluid ^{3}He-B," *J. Low Temp. Phys.*, vol. 122, no. 5/6, 2001.

[46] V. V. Dmitriev, I. V. Kosarev, M. Krusius, D. V. Ponarin, V. M. H. Ruutu, and G. E. Volovik, "Stable spin precession at one half of equilibrium magnetization in superfluid ^{3}He-B," *Phys. Rev. Lett.*, vol. 78, pp. 86–89, Jan. 1997.

[47] V. V. Dmitriev, I. V. Kosarev, and D. V. Ponarin, "Observation of fractional harmonics in the NMR signal from superfluid ^{3}He-B," *JETP Lett.*, vol. 69, pp. 215–220, Feb. 1999.

[48] Y. Kondo, J. S. Korhonen, M. Krusius, V. V. Dmitriev, Yu. M. Mukharsky, E. B. Sonin, and G. E. Volovik, "Direct observation of the nonaxisymmetric vortex in superfluid ^{3}He-B," *Phys. Rev. Lett.*, vol. 67, pp. 81–84, July 1991.

[49] Y. Kondo, J. S. Korhonen, M. Krusius, V. V. Dmitriev, E. V. Thuneberg, and G. E. Volovik, "Combined spin-mass vortex with soliton tail in superfluid ^{3}He-B," *Phys. Rev. Lett.*, vol. 68, pp. 3331–3334, June 1992.

[50] I. A. Fomin, "Solution of spin dynamics equations for ^{3}He superfluid phases in a strong magnetic field," *J. Low Temp. Phys.*, vol. 31, pp. 509–526, May 1978.

[51] N. D. Mermin and T.-L. Ho, "Circulation and angular momentum in the A phase of superfluid helium-3," *Phys. Rev. Lett.*, vol. 36, pp. 594–597, Mar. 1976.

[52] J. M. Karimäki and E. V. Thuneberg, "Periodic vortex structures in superfluid ^{3}He-A," *Phys. Rev. B*, vol. 60, pp. 15290–15301, Dec. 1999.

[53] P. J. Hakonen, O. T. Ikkala, and S. T. Islander, "Experiments on vortices in rotating superfluid ^{3}He-A," *Phys. Rev. Lett.*, vol. 49, pp. 1258–1261, Oct. 1982.

[54] H. K. Seppälä and G. E. Volovik, "Evidence for nonsingular vorticity in the Helsinki experiments on rotating ^{3}He-A," *J. Low Temp. Phys.*, vol. 51, pp. 279–290, May 1983.

[55] V. M. H. Ruutu, J. Kopu, M. Krusius, Ü. Parts, B. Plaçais, E. V. Thuneberg, and W. Xu, "Critical velocity of vortex nucleation in rotating superfluid ^{3}He-A," *Phys. Rev. Lett.*, vol. 79, pp. 5058–5061, Dec. 1997.

[56] Ü. Parts, Y. Kondo, J. S. Korhonen, M. Krusius, and E. V. Thuneberg, "Vortex layer on the interface between the A and B phases in superfluid ^{3}He," *Phys. Rev. Lett.*, vol. 71, pp. 2951–2954, Nov. 1993.

[57] E. V. Thuneberg, "Some considerations on the equilibrium A-B interface," *Physica B*, vol. 178, pp. 168–175, 1992.

[58] D. D. Osheroff and M. C. Cross, "Interfacial surface energy between the superfluid phases of He^3," *Phys. Rev. Lett.*, vol. 38, pp. 905–909, Apr. 1977.

[59] D. S. Buchanan, G. W. Swift, and J. C. Wheatley, "Velocity of propagation of the ^{3}He A-B interface in hypercooled ^{3}He-A," *Phys. Rev. Lett.*, vol. 57, pp. 341–344, July 1986.

[60] E. V. Thuneberg, Ü. Parts, Y. Kondo, J. S. Korhonen, and M. Krusius, "Quantized vortices at a moving A-B interface in superfluid ^{3}He," *Physica B*, vol. 194–196, pp. 779–780, 1994.

[61] M. Krusius, E. V. Thuneberg, and Ü. Parts, "A-B phase transition in rotating superfluid ^{3}He," *Physica B*, vol. 197, pp. 376–389, 1994.

[62] T. W. B. Kibble, "Topology of cosmic domains and strings," *J. Phys. A: Math. Gen.*, vol. 9, pp. 1387–1398, Aug. 1976.

[63] G. Dvali, J. Liu, and T. Vachaspati, "Sweeping away the monopole problem," *Phys. Rev. Lett.*, vol. 80, pp. 2281–2284, Mar. 1998.

[64] L. Pogosian and T. Vachaspati, "Interaction of magnetic monopoles and domain walls," *Phys. Rev. D*, vol. 62, pp. 105005–1–4, Nov. 2000.

[65] D. J. Cousins, M. P. Enrico, S. N. Fisher, S. L. Phillipson, G. R. Pickett, N. S. Shaw, and P. J. Y. Thibault, "Probing the A-B phase interface in superfluid ^{3}He by Andreev reflection of a quasiparticle beam," *Phys. Rev. Lett.*, vol. 77, pp. 5245–5248, Dec. 1996.

[66] M. Bartkowiak, S. W. J. Daley, S. N. Fisher, A. M. Guénault, G. N. Plenderleith, R. P. Haley, G. R. Pickett, and P. Skyba, "Thermodynamics of the A-B phase transition and the geometry of the A-phase gap nodes in superfluid ^{3}He at low temperatures," *Phys. Rev. Lett.*, vol. 83, pp. 3462–3465, Oct. 1999.

[67] S. N. Fisher, A. M. Guénault, R. P. Haley, G. R. Pickett, G. N. Plenderleith, and P. Skyba, "Measurements on a dynamic A-B phase boundary in superfluid ^{3}He at very low temperatures," *J. Low Temp. Phys.*, vol. 113, pp. 651–659, Dec. 1998.

[68] M. Bartkowiak, S. N. Fisher, A. M. Guénault, R. P. Haley, G. R. Pickett, G. N. Plenderleith, and P. Skyba, "Primary and secondary nucleation of the transition between the A and B phases of superfluid ^{3}He," *Phys. Rev. Lett.*, vol. 85, pp. 4321–4324, Nov. 2000.

[69] R. Kaul and H. Kleinert, "Surface energy and textural boundary conditions between A and B phases of ^{3}He," *J. Low Temp. Phys.*, vol. 38, pp. 539–552, Mar. 1980.

[70] S. Yip, "Quasiparticle motion in superfluid ^{3}He and Kapitza resistance of ^{3}He A-B phase boundary," *Phys. Rev. B*, vol. 32, pp. 2915–2928, Sept. 1985.

[71] S. Yip and A. J. Leggett, "Dynamics of the ^{3}He A-B boundary," *Phys. Rev. Lett.*, vol. 57, pp. 345–348, July 1986.

[72] M. M. Salomaa, "Monopoles in the rotating superfluid helium-3 A–B interface," *Nature*, vol. 326, pp. 367–730, Mar. 1987.

[73] N. Schopohl, "Spatial dependence of the order parameter of superfluid ^{3}He at the A-B phase boundary," *Phys. Rev. Lett.*, vol. 58, pp. 1664–1667, Apr. 1987.

[74] S. Yip, "Symmetry considerations and physical properties of the order parameter of the ^{3}He A-B interface," *Phys. Rev. B*, vol. 35, pp. 8733–8736, June 1987.

[75] M. M. Salomaa, "A phase transition of the moving superfluid ^{3}He A-B interface," *J. Phys. C: Solid State Phys.*, vol. 21, pp. 4425–4435, 1988.

[76] E. V. Thuneberg, "A-B interface of superfluid ^{3}He in a magnetic field," *Phys. Rev. B*, vol. 44, pp. 9685–9691, Nov. 1991.

[77] G. E. Volovik, "AB interface in superfluid ^{3}He and Casimir effect," *JETP Lett.*, vol. 63, pp. 483–489, 1996. cond-mat/9602129.

[78] I. Hahn, *Thermodynamic study of the A-B phase transition in superfluid ^{3}He: Phase diagram and consequences.* PhD thesis, University of Southern California, May 1993.

[79] P. J. Hakonen, M. Krusius, M. M. Salomaa, R. H. Salmelin, J. T. Simola, A. D. Gongadze, G. E. Vachnadze, and G. A. Kharadze, "NMR and axial magnetic field textures in stationary and rotating superfluid ^{3}He-B," *J. Low Temp. Phys.*, vol. 76, no. 3/4, pp. 225–283, 1989.

[80] P. Schiffer, M. T. O'Keefe, M. D. Hildreth, H. Fukuyama, and D. D. Osheroff, "Strong supercooling and stimulation of the A-B transition in superfluid ^{3}He," *Phys. Rev. Lett.*, vol. 69, pp. 120–123, July 1992.

[81] F. Pobell, *Matter and Methods at Low Temperatures*. Berlin / Heidelberg: Springer-Verlag, 1992.

[82] J. Koivuniemi, R. Luusalo, and P. Hakonen, "Bipolar programmable current supply for superconducting nuclear magnetic resonance magnets," *Rev. Sci. Instrum.*, vol. 69, pp. 3418–3425, Sept. 1998.

[83] J. P. Pekola, K. Torizuka, A. J. Manninen, J. M. Kyynäräinen, and G. E. Volovik, "Observation of a topological transition in the ^{3}He-A vortices," *Phys. Rev. Lett.*, vol. 65, pp. 3293–3296, Dec. 1990. Errata: vol. 67, p. 1055, Aug. 1991.

[84] M. M. Salomaa and G. E. Volovik, "Quantized vortices in superfluid ^{3}He," *Rev. Mod. Phys.*, vol. 59, pp. 533–613, July 1987. Erratum: vol. 60, p. 573, Apr. 1988.

[85] Ü. Parts, E. V. Thuneberg, G. E. Volovik, J. H. Koivuniemi, V. M. H. Ruutu, M. Heinilä, J. M. Karimäki, and M. Krusius, "Vortex sheet in rotating superfluid ^{3}He-A," *Phys. Rev. Lett.*, vol. 72, pp. 3839–3842, June 1994.